Biomaterials 112 (2017) 44–61

Contents lists available at ScienceDirect

Biomaterials

journal homepage: www.elsevier.com/locate/biomaterials

'Dual' peptidyl-oligonucleotide conjugates: Role of conformational flexibility in catalytic cleavage of RNA

Yaroslav Staroseletz [b, 1], Aled Williams [a, 1], Kepa K. Burusco [a], Irfan Alibay [a], Valentin V. Vlassov [b], Marina A. Zenkova [b], Elena V. Bichenkova [a, *]

[a] School of Health Sciences, Faculty of Biology, Medicine and Health, University of Manchester, Oxford Road, Manchester, M13 9PT, UK
[b] Institute of Chemical Biology and Fundamental Medicine SB RAS, 8 Laurentiev Avenue, 630090, Novosibirsk, Russia

ARTICLE INFO

Article history:
Received 16 August 2016
Received in revised form
23 September 2016
Accepted 26 September 2016
Available online 3 October 2016

Keywords:
RNA cleavage
Peptidyl-oligonucleotide conjugate
Supramolecular self-assembly
Hybridization
Conformation

ABSTRACT

Traditional therapeutic interventions against abnormal gene expression in disease states at the level of expressed proteins are becoming increasingly difficult due to poor selectivity, off-target effects and associated toxicity. Upstream catalytic targeting of specific RNA sequences offers an alternative platform for drug discovery to achieve more potent and selective treatment through antisense interference with disease-relevant RNAs. We report a novel class of catalytic biomaterials, comprising amphipathic RNA-cleaving peptides placed between two RNA recognition motifs, here demonstrated to target the TΨC loop and 3′- acceptor stem of $tRNA^{Phe}$. These unique peptidyl-oligonucleotide 'dual' conjugates (DCs) were created by phosphoramidate or thiol-maleimide conjugation chemistry of a TΨC-targeting oligonucleotide to the *N*-terminus of the amphipathic peptide sequence, followed by amide coupling of a 3′-acceptor stem-targeting oligonucleotide to the free C-terminal carboxylic acid functionality of the same peptide. Hybridization of the DCs bearing two spatially-separated recognition motifs with the target $tRNA^{Phe}$ placed the peptide adjacent to a single-stranded RNA region and promoted cleavage within the 'action radius' of the catalytic peptide. Up to 100% cleavage of the target $tRNA^{Phe}$ was achieved by the best candidate (*i.e.* DC6) within 4 h, when conformational flexibility was introduced into the linker regions between the peptide and oligonucleotide components. This study provides the strong position for future development of highly selective RNA-targeting agents that can potentially be used for disease-selective treatment at the level of messenger, micro, and genomic viral RNA.

1. Introduction

RNA-targeting agents are recognized as a promising alternative to conventional small-molecule therapeutic strategies, suffering from poor target selectivity, as a result of their small size and the limited number of chemical functional groups available in low molecular weight drugs. Poor selectivity may ultimately lead to toxicity and other off-target effects undesirable in humans [1,2]. Silencing disease-specific genes at the level of expressed RNA may offer an opportunity to reduce these undesirable drug-related side effects, commonly associated with poor drug selectivity and/or the high dosages necessary to achieve a therapeutic effect. Also, the traditional drug discovery process against pathogenic proteins requires laborious virtual and/or experimental screening of numerous drug leads against each target. In contrast, the development of RNA therapies is facilitated by a logical and common design platform of antisense targeting based on a highly-predictable 3D structural organisation of nucleic acids. Moreover, RNA-targeting interventions may be extended to a number of other biologically-significant RNAs (*e.g.,* miRNAs), which are implicated in many pathological disease processes, including various types of cancer (breast [3], ovarian [4], lung cancer [5]), cardiovascular [6,7] and neurodegenerative diseases [8]. Potential targets also include messenger-RNA transcripts (*e.g.,* mRNA encoding clusterin, an anti-apoptotic chaperone protein upregulated in cancer cells [9,10]) or viral-genomic RNAs (*e.g.,* HIV [11,12] or Ebola [13,14]). Sequence-specific targeting at the RNA level may considerably reduce the

Abbreviations: ASO, antisense oligonucleotide; DC, dual conjugate; POC, peptidyl-oligonucleotide conjugate; FITC, fluorescein isothiocyanate; MALDI, matrix-assisted laser desorption ionization); nt, nucleotide; RT, room temperature; TSP, trimethylsilyl propanoic acid.

* Corresponding author.
E-mail address: Elena.V.Bichenkova@manchester.ac.uk (E.V. Bichenkova).

[1] Yaroslav Staroseletz and Aled Williams contributed equally to the work.

http://dx.doi.org/10.1016/j.biomaterials.2016.09.033

discovery costs associated with target identification and validation of pathological proteins, and the associated subsequent lengthy process of lead identification using ligand-, mechanism- or receptor-based rational drug design.

Currently, siRNA and antisense oligonucleotides (ASO) are the two main approaches to target disease at the level of messenger RNA. The discovery of siRNA in 1999 [15] led to the incorporation of a number of specialist biotechnology companies (*e.g.,* Sirna Therapeutics, Dicerna Pharmaceuticals, Alnylam Pharmaceuticals, Sirnaomics Inc.). However, various issues persist and prevent the translation of siRNA into the clinic including: (i) undesirable immune responses triggered by siRNA [16–18], (ii) saturation of the RNA-induced silencing-complex (RISC) [19] leading to upregulation of disease causing proteins, and (iii) poor cellular delivery [18,20–22]. This has led to a number of large pharmaceutical companies discontinuing their siRNA research and development pipeline [23]. Antisense oligonucleotides on the other hand have reached clinical application for a number of treatments including Fomivirsen [24] (Vitravene®) for the treatment of cytomegalovirus retinitis and Mipomersen [25] (Kynamro®) for homozygous familial hypercholesterolemia. However, their mechanism of action is often based on a 1:1 binding stoichiometry and thus requires a relatively high dosage of ASO to silence the target mRNA transcript effectively [26].

An alternative approach for irreversible targeting of RNA sequences is based on the use of artificial (or chemically-engineered) ribonucleases. This class of supramolecular biomaterials is designed to mimic the active centres of natural enzymes to be capable of accelerating the spontaneous, irreversible degradation of the RNA phosphodiester backbone. Peptidyl-oligonucleotide conjugates (POCs) are a particular class of chemical ribonucleases, which catalyse the hydrolytic cleavage of the RNA phosphodiester backbone [27–30]. POCs typically consist of a short (*e.g.,* 6 to 17-mer) targeting motif and a covalently-attached amphiphilic peptide (5–10-mer) with alternating leucine and arginine residues. The antisense motif is able to target a specific RNA and direct the catalytic peptide to the desired RNA region, thus increasing its effective concentration in the vicinity of the cleavage site. The overall cationic nature of the peptide sequence, due to the presence of arginine residues, allows it to interact with the negatively-charged phosphodiester backbone within the target RNA region, and to promote RNA hydrolysis without the need for exogenous species such as enzymes or cofactors (*e.g.,* RISC, RNase H).

Recently, we demonstrated [30] complete site-selective cleavage of model RNA (yeast $tRNA^{Phe}$) under physiological conditions over a 12–24 h period without the need for exogenous species (*e.g.,* metal ions, additional enzymes) and at POC:RNA concentration ratio of 20:1. The artificial ribonucleases there were constructed from peptidyl-oligonucleotide conjugates (POCs) containing a short amphiphilic peptide sequence (consisting of leucine, arginine and glycine amino acid residues) and a 17-mer oligodeoxynucleotide recognition fragment (GATCGAACACAGGACCT), which were coupled together chemically by a phosphoramidate bond between the peptide *N*-terminus and the 5′-terminal phosphate group. Notably, RNA cleavage was observed only when the peptide and oligonucleotide constituents were covalently attached to form a catalytically-active peptidyl-oligonucleotide conjugate. A significant discovery of this study [30] and some previous investigations [28,31] is that the structural properties of the joint molecular blocks and their molecular flexibility influenced the functional performance of these supramolecular catalysts, and thus should be considered in the future design of novel chemical ribonucleases. In order for peptide-mediated RNA-cleavage to occur, the peptide must adopt a conformation which can enhance the natural spontaneous hydrolysis of RNA [32,33]. Accordingly, this report considers whether increasing the flexibility of the peptide at the point of its restriction (*i.e.,* at the rigid oligonucleotide motif in its hybridised double-stranded state) favours the number of non-covalent interactions, with the target RNA sequence, to promote the required 'in-line' geometry necessary for 2′OH attack of the bridging phosphorus atom.

Herein, we designed and synthesized such a new generation of POCs, which places the catalytic peptide in-between two oligodeoxynucleotide recognition motifs (see Fig. 1). In order to investigate the role of conformational flexibility on the hybridization properties and catalytic performance of these conjugates against RNA, we varied the structure and length of the linker groups and recognition motifs. These novel 'dual' conjugates were targeted towards the TΨC loop and 3′- overhang of yeast $tRNA^{Phe}$. Although not a clinically relevant RNA target, $tRNA^{Phe}$ contains many of the secondary structural elements present in messenger-, micro- or viral-RNA sequences and, therefore, serves well as a *proof of concept* target for the development of these novel DCs. Furthermore, many chemical nucleases have been validated against this target, allowing direct comparison of RNA cleavage activity with other work [31,34]. Through chemical modification of peptide *N*- and *C*-termini with 3′- or 5′- modified oligodeoxynucleotides, a library of 11 novel dual conjugates (DCs) have been synthesized, isolated and fully characterized. We present here their RNA hybridization and cleavage properties against $tRNA^{Phe}$ under physiological conditions and report a remarkably high RNA cleavage activity of the best structural variant of the DCs.

2. Materials and methods

2.1. Chemicals, reagents and facilities

Reagents and materials were purchased from Sigma-Aldrich (UK), unless otherwise indicated. Oligodeoxynucleotides were purchased from AtdBio Ltd. (Southampton, UK). Fmoc-Gly-Rink Amide-MBHA peptide resin was purchased from Eurogentec Ltd. (Liège, Belgium). T7 RNA polymerase and plasmid p67YF0 were kindly provided by Dr. S. Khodyreva and Dr. N. Moor, respectively (Institute of Chemical Biology and Fundamental Medicine, Siberian Branch of the Russian Academy of Sciences). RNase T1 was purchased from Fermentas (Lithuania), and restriction enzymes Bst2UI and Fok1 were purchased from SibEnzyme Ltd. (Russian Federation). pHIV-1 was kindly provided by Prof. H.J. Gross (University of Würzburg, Germany).

Purification of peptides and peptidyl-oligonucleotide conjugates were performed using Agilent 1100 HPLC system (Agilent Technologies, Santa Clara, CA). Reversed phase chromatography was carried out in a similar way as described earlier [30] using a semi-preparative column Luna C18 (Phenomenex; CA, USA). Ion-exchange chromatography (IEX) purifications of dual-conjugates were carried out using a Clarity Oligo-WAX (150 × 4.6 mm, 10 Å pore size, Phenomenex; CA, USA) column. Mass spectrometry service was kindly provided by EPSRC National Mass Spectrometry Centre (Swansea, UK). Some MALDI mass spectra of 'mono' and 'dual' peptidyl-oligonucleotide conjugates were recorded using a Bruker Daltonics Ultraflex TOF/TOF mass spectrometer (MA, USA) at Manchester Institute of Biotechnology (Manchester, UK) using the method described earlier in Ref. [30]. ^{1}H and ^{31}P NMR spectra were recorded using Bruker Avance II+ 400 NMR spectrometer (400 MHz) equipped with TopSpin 3.2 software for NMR data acquisition and processing.

2.2. Peptide synthesis, purification and characterization

Peptides $[LR]_2G$, $[LR]_3G$, $[LR]_4G$, Mal-$[LR]_4G$ and Mal-$[LRLRG]_2$

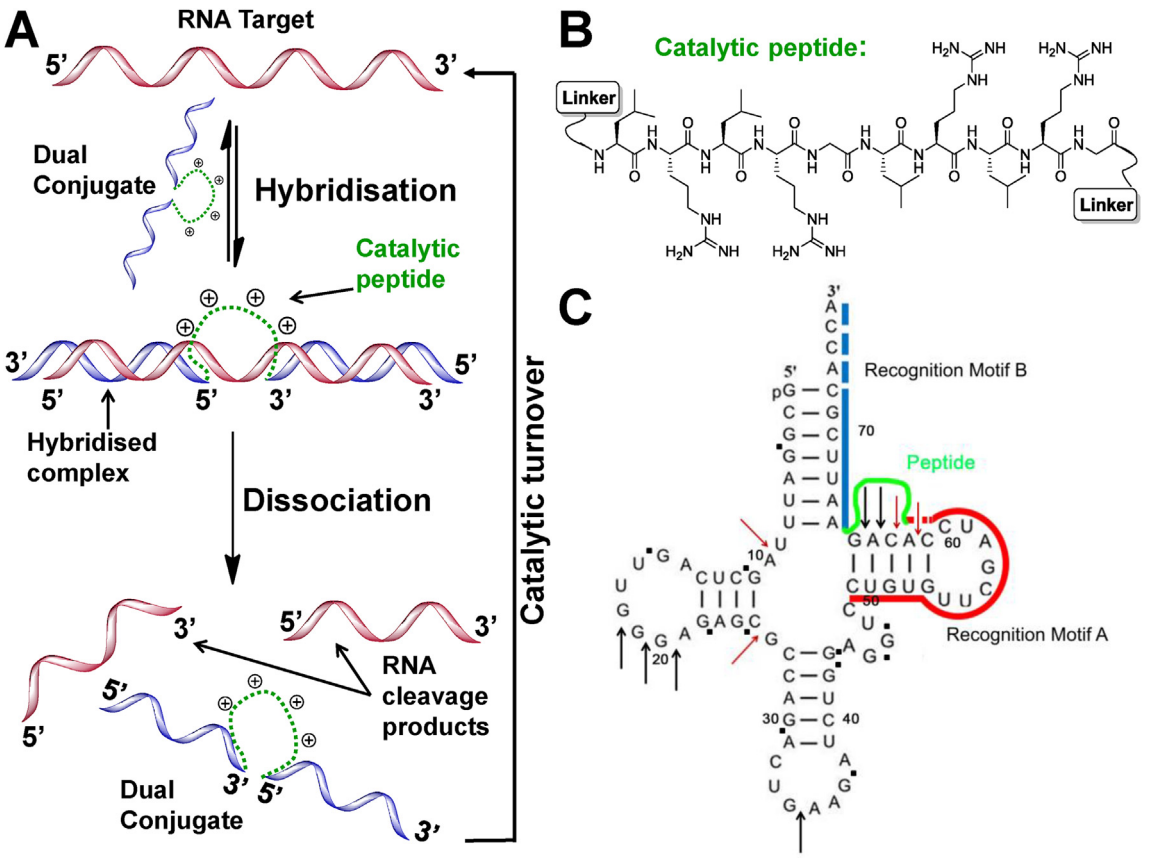

Fig. 1. A. Design concept of 'dual' peptidyl-oligonucleotide conjugate, which incorporates catalytic peptide (green) as a linker between two oligodeoxyribonucleotide recognition motifs. **B**. Representative structure of the catalytic peptide incorporated into 'dual' conjugates DC4-DC6 and DC8-DC11, containing $[Leu\text{-}Arg]_n$ building blocks. **C**. Secondary structure of $tRNA^{Phe}$ (*in-vitro* transcript) along with the TΨC- and acceptor stem binding sites targeted by Recognition Motif A (red) and B (blue), respectively. Solid lines represent regions targeted by all recognition motifs. Dotted lines show regions targeted by extended recognition motifs as listed in Table 1. The peptide (green) connecting Recognition Motifs A and B reside close to the $^{65}GACAC^{61}$ target sequence. Red arrows show cleavage sites induced in $tRNA^{Phe}$ by DC7, whereas black arrows and black squares show major and minor cleavage sites, respectively, induced by DC6.

were synthesized and purified according to a previously reported protocol [30]. *N*-terminal maleimide modification was achieved with *N*-maleoyl-β-alanine (101 mg, 0.6 mmol) using the coupling conditions identical to those described in Ref. [30].

Analytical data for $[LR]_2G$ and $[LR]_4G$ peptides acquired from mass spectrometry and ^1H NMR has been previously reported [30] (see data for (**5**) and (**4**), respectively).

2.2.1. $[LR]_3G$

(188 mg, yield 70%). ESI-MS: $m/z = 442.3$ for $[M+2H]^{2+}$, 295.2 for $[M+3H]^{3+}$ (MW = 882.59 calcd. for $[C_{38}H_{74}N_{16}O_8]$). ^1H NMR (D_2O with TSP (0.1 μM), 400 MHz): δ 0.87–0.96 (m, 18H, Leu-H^{δ}), 1.51–1.96 (m, 21H, Leu-$H^{\beta,\gamma}$, Arg-$H^{\beta,\gamma}$), 3.18–3.23 (s, 6H, Arg-H^{δ}), 3.82 (s, 2H, Gly-H), 4.02 (t, 1H, $J = 10.12$ Hz, *N*-Leu-H^{α}), 4.31–4.42 (m, 5H, Leu/Arg-H^{α}).

2.2.2. Mal-$[LR]_4G$

(250 mg, yield 70%). ESI-MS: $m/z = 652.4$ for $[M+2H]^{2+}$, 435.3 for $[M+3H]^{3+}$ (MW = 1302.80 calcd. for $[C_{57}H_{102}N_{22}O_{13}]$). ^1H NMR (D_2O with TSP (0.1 μM), 400 MHz): δ 0.87–0.96 (m, 24H, Leu-H^{δ}), 1.50–1.91 (m, 28H, 8 × Arg-H^{β}, 8 × Arg-H^{γ}, 8 × Leu-H^{β}, 4 × Leu-H^{γ}), 2.42–2.66 (m, 2H, Mal-H^{β}), 3.16–3.24 (m, 8H, Arg-H^{δ}), 3.73–3.90 (m, 2H, Mal-H^{α}) 3.86–4.44 (m, 10H, 2 × Gly-H, 8 × Leu/Arg-H^{α}), 6.82 (s, 2H, Mal-H).

2.2.3. Mal-$[LRLRG]_2$

(260 mg, yield 72%). ESI-MS: $m/z = 680.9$ for $[M+2H]^{2+}$, 454.3 for $[M+3H]^{3+}$ (MW = 1359.82 calcd. for $[C_{59}H_{105}N_{23}O_{14}]$). ^1H NMR (D_2O with TSP (0.1 μM), 400 MHz): δ 0.84–0.95 (m, 24H, Leu-H^{δ}), 1.45–1.91 (m, 28H, 8 × Arg-H^{β}, 8 × Arg-H^{γ}, 8 × Leu-H^{β}, 4 × Leu-H^{γ}), 2.46–2.65 (m, 2H, Mal-H^{β}), 3.18–3.24 (m, 8H, Arg-H^{δ}), 3.71–3.87 (m, 2H, Mal-H^{α}) 3.90–4.39 (m, 12H, 4 × Gly-H, 8 × Leu/Arg-H^{α}), 6.86 (s, 2H, Mal-H).

2.3. Single conjugate synthesis (Method 1)

In order to attach peptide $[LR]_2G$, $[LR]_3G$ or $[LR]_4G$ to oligonucleotide pGATCGAACACAG (**1**) containing 5′-terminal phosphate group we used Method 1, which was an adaptation of the previously described protocol [30] for conjugation of 5′-phosphate modified oligonucleotides with peptides containing free *N*-terminal amine groups (see Scheme S1, 'Supplementary Data').

2.4. Single conjugate synthesis (Method 2)

Thiol (disulphide protected) modified oligonucleotide, *Thiol*-GATCGAACACAG (**2**), *Thiol*-GGATCGAACACAG (**3**) or Thiol-TGGATCGAACACAG (**4**) (0.12 μmol) in phosphate-buffered saline at pH 7 (200 μL) was reduced by addition of 3% (w/v) *tris*(2-carboxyethyl)phosphine (TCEP; 12 μL) and shaken for 1 h. The pH was then adjusted to pH 7 with NaOH (0.5 M). Maleimide-modified

peptide, Mal-[LR]$_4$G or Mal-[LRLRG]$_2$ (1.2 μmol), was dissolved in a minimal volume of DMSO (≈15 μL) and added dropwise to the oligonucleotide solution with gentle agitation (see Scheme S2, 'Supplementary Data'). The reactions were mechanically shaken for 2 h at RT. The conjugation product along with the starting oligonucleotide was precipitated with $LiClO_4$ (4% w/v in acetone) as described in detail in Ref. [30]. Before attachment of the second oligonucleotide motif, the 'single' conjugates were purified by RP-HPLC in a similar way described earlier in Ref. [30].

2.5. Dual conjugate synthesis

Single conjugate (0.1 μmol) dissolved in 0.1 M 2-(*N*-morpholino) ethanesulfonic acid buffer pH 6 (MES; 50 μL) was mixed with an equal quantity (0.1 μmol) of aminohexyl-modified oligonucleotide (oligonucleotides **5**, **6**, **7**, **8** or **9**) dissolved in MES (20 μL), *N*-hydroxysuccinimide (NHS; 0.16 μmol) and 1-ethyl-3-(3-dimethylaminopropyl)carbodiimide (EDC; 1.6 μmol) (see Scheme S3, 'Supplementary Data'). The reaction mixtures were left overnight at RT, when they were diluted to 1 mL with 0.05 M $LiClO_4$ and purified directly by IEX (see below) or by RP-HPLC as described earlier in Ref. [30].

2.6. Dual conjugate purification by IEX

Conjugates were purified by IEX directly from reaction mixtures. The flow rate was maintained at 2.0 mL/min using 10 mM Tris-Cl (pH 7.25) and 10% AcCN as eluent A and 10 mM Tris-Cl (pH 7.25), 2 M NaCl and 10% AcCN as eluent B. The absorbance was monitored at 260 nm and the following gradient was applied: 100% A for 2 min, 0% B to 80% B in 18 min for DC1 - DC3; 100% A for 3 min, 0% B to 100% B in 23 min for DC8 - DC9; 100% A for 5 min, 0% B to 100% B in 32 min for DC4 - DC7, DC10 - DC11. Product peaks were collected and then desalted using RP-HPLC with 0.05 M $LiClO_4$ as eluent A and 0.05 M $LiClO_4$ in AcCN as eluent B. The absorbance was monitored at 260 nm and the following gradient was applied: 100% A for 3 min, 0% B to 100% B in 10 min. Product peaks were collected, freeze-dried and combined. The excess salt was removed by dissolving the material in H_2O (100 μL) and precipitating in 4% $LiClO_4$ in acetone (w/v) (1.8 mL) overnight. The product was collected by centrifugation (13400 rpm, 4 min), air-dried and then freeze-dried.

2.7. Dual conjugate characterization

Identity and purity of all 'dual' peptidyl-oligonucleotide conjugates have been confirmed by IEX or RP-HPLC, Urea-PAGE (Fig. S1, 'Supplementary Data'), ^{31}P and/or ^{1}H NMR spectroscopy (Fig. 3 and Fig. S2, 'Supplementary Data') and mass spectrometry (Fig. S3, 'Supplementary Data'). ^{1}H NMR analysis was carried out on all DCs; however, the H3′/H4′/H5′/H5″ sugar ring proton regions (3.5–5.0 ppm) were not analysed due to suppression of residual water signal at 4.8 ppm. ^{31}P NMR analysis was carried out only on DCs 1, 2 and 3 since it cannot be used as a characterization tool for DCs 4 to 11 due to the nature of 5′-thiol modification. Urea-PAGE analysis of the synthesized DCs illustrates their purity (98–100%.) and reduced electrophoretic mobility versus the intermediate 'single' POCs and unconjugated oligonucleotide (see Fig. S1 in the 'Supplementary Data'). Mass spectrometry analysis of DCs was carried out using matrix-assisted laser desorption ionization spectroscopy (MALDI). DCs were identified as mono- or di-sodium/potassium adducts with experimental masses in agreement with theoretical calculations.

2.7.1. DC1 ($^{5'}$ **1**-[LR]$_2$G-**5** $^{3'}$)

(67 nmol, yield 67%). MALDI-MS: m/z = 7914 $[M+H]^+$ (MW = 7913 calcd. for $[C_{259}H_{347}N_{104}O_{143}P_{23}]$). ^{1}H NMR ($D_2O$ with TSP (0.01 μM), 400 MHz): δ 0.62–0.93 (m, 12H, Leu-H$^{\delta}$), 1.14–3.16 (m, 92H, 23 × H2′ and 23 × H2″ sugar ring protons, 5 × CH_3 of 5 × dT, 4×Arg-H$^{\beta}$, 4 × Arg-H$^{\delta}$, 4 × Arg-H$^{\gamma}$, 4 × Leu-H$^{\beta}$, 2 × Leu-H$^{\gamma}$, 6 × CH_2 (aminohexyl linker), 1 × CH (aminohexyl linker)), 5.32–6.33 (m, 27H, 23 × H1′ sugar ring protons, 4 × H5 of dC), 7.25–8.28 (m, 30H, 30 × Ar-H from dG(× 7), dA(× 14), dC(× 4) and dT(× 5)). ^{31}P{^{1}H} NMR (D_2O, 160 MHz): δ −1.50 to −0.39 (22P, PO_4), 6.13 (1P, *N*-PO_3). No sample reference was used for ^{31}P NMR analysis. It was carried out to observe the relative shift of the ^{31}P-N resonance.

2.7.2. DC2 ($^{5'}$ **1**-[LR]$_3$G-**5** $^{3'}$)

(86 nmol, yield 86%). MALDI-MS: m/z = 8184 $[M+H]^+$ (MW = 8183 calcd. for $[C_{271}H_{370}N_{109}O_{145}P_{23}]$). ^{1}H NMR ($D_2O$ with TSP (0.01 μM), 400 MHz): δ 0.61–0.91 (m, 18H, Leu-H$^{\delta}$), 1.14–3.18 (m, 101H, 23 × H2′ and 23 × H2″ sugar ring protons, 5 × CH_3 of 5 × dT, 6×Arg-H$^{\beta}$, 6 × Arg-H$^{\delta}$, 6 × Arg-H$^{\gamma}$, 6 × Leu-H$^{\beta}$, 3 × Leu-H$^{\gamma}$, 6 × CH_2 (aminohexyl linker), 1 × CH (aminohexyl linker)), 5.36–6.31 (m, 27H, 23 × H1′ sugar ring protons, 4 × H5 of dC), 7.25–8.34 (m, 30H, 30 × Ar-H from dG(× 7), dA(× 14), dC (× 4) and dT (× 5)). ^{31}P{^{1}H} NMR (D_2O, 160 MHz): δ −1.54 to −0.41 (22P, PO_4), 5.86 (1P, *N*-PO_3). No sample reference was used for ^{31}P NMR analysis. It was carried out to observe the relative shift of the ^{31}P-N resonance.

2.7.3. DC3 ($^{5'}$ **1**-[LR]$_4$G-**5** $^{3'}$)

(71 nmol, yield 71%). MALDI-MS: m/z = 8453 $[M+H]^+$ (MW = 8452 calcd. for $[C_{283}H_{393}N_{114}O_{147}P_{23}]$). ^{1}H NMR ($D_2O$ with TSP (0.01 μM), 400 MHz): δ 0.52–0.86 (m, 24H, Leu-H$^{\delta}$), 1.07–3.15 (m, 110H, 23 × H2′ and 23 × H2″ sugar ring protons, 5 × CH_3 of 5 × dT, 8×Arg-H$^{\beta}$, 8 × Arg-H$^{\delta}$, 8 × Arg-H$^{\gamma}$, 8 × Leu-H$^{\beta}$, 4 × Leu-H$^{\gamma}$, 6 × CH_2 (aminohexyl linker), 1 × CH (aminohexyl linker)), 5.29–6.25 (m, 27H, 23 × H1′ sugar ring protons, 4 × H5 of dC), 7.19–8.29 (m, 30H, 30 × Ar-H from dG(× 7), dA(× 14), dC(× 4) and dT(× 5)). ^{31}P{^{1}H} NMR (D_2O, 160 MHz): δ −1.79 to −0.71 (22P, PO_4), 5.92 (1P, *N*-PO_3). No sample reference was used for ^{31}P NMR analysis. It was carried out to observe the relative shift of the ^{31}P-N resonance.

2.7.4. DC4 ($^{5'}$ **4**-Mal-[LRLRG]$_2$–**5** $^{3'}$)

(67 nmol, yield 67%). MALDI-MS: m/z = 9430 $[M+H]^+$ (MW = 9429 calcd. for $[C_{318}H_{440}N_{123}O_{165}P_{25}S]$). ^{1}H NMR ($D_2O$ with TSP (0.01 μM), 400 MHz): δ 0.72–0.89 (m, 24H, Leu-H$^{\delta}$), 1.15–3.24 (m, 131H, 25 × H2′ and 25 × H2″ sugar ring protons, 6 × CH_3 of 6 × dT, 8×Arg-H$^{\beta}$, 8 × Arg-H$^{\delta}$, 8 × Arg-H$^{\gamma}$, 8 × Leu-H$^{\beta}$, 4 × Leu-H$^{\gamma}$, 6 × CH_2 (aminohexyl linker), 1 × CH (aminohexyl linker), 6 × CH_2 (thiohexyl linker), 2 × Mal-H$^{\beta}$), 5.40–6.33 (m, 29H, 25 × H1′ sugar ring protons, 4 × H5 of dC), 7.25–8.35 (m, 32H, 32 × Ar-H from dG(× 8), dA(× 14), dC(× 4) and dT(× 6)).

2.7.5. DC5 ($^{5'}$ **3**-Mal-[LRLRG]$_2$–**5** $^{3'}$)

(79 nmol, yield 79%). MALDI-MS: m/z = 9167 $[M+H+ACN]^+$ (MW = 9125 calcd. for $[C_{308}H_{427}N_{121}O_{158}P_{24}S]$). ^{1}H NMR ($D_2O$ with TSP (0.01 μM), 400 MHz): δ 0.72–0.89 (m, 24H, Leu-H$^{\delta}$), 1.15–3.24 (m, 126H, 24 × H2′ and 24 × H2″ sugar ring protons, 5 × CH_3 of 5 × dT, 8×Arg-H$^{\beta}$, 8 × Arg-H$^{\delta}$, 8 × Arg-H$^{\gamma}$, 8 × Leu-H$^{\beta}$, 4 × Leu-H$^{\gamma}$, 6 × CH_2 (aminohexyl linker), 1 × CH (aminohexyl linker), 6 × CH_2 (thiohexyl linker), 2 × Mal-H$^{\beta}$), 5.40–6.33 (m, 28H, 24 × H1′ sugar ring protons, 4 × H5 of dC), 7.25–8.35 (m, 31H, 31 × Ar-H from dG(× 8), dA(× 14), dC(× 4) and dT(× 5)).

2.7.6. DC6 ($^{5'}$ **2**-Mal-[LRLRG]$_2$-**5** $^{3'}$)

(70 nmol, yield 70%). MALDI-MS: m/z = 8797 $[M+H]^+$ (MW = 8796 calcd. for $[C_{298}H_{415}N_{116}O_{152}P_{23}S]$). ^{1}H NMR ($D_2O$ with

TSP (0.01 μM), 400 MHz): δ 0.70–0.99 (m, 24H, Leu-H^{δ}), 1.25–3.25 (m, 124H, 23 × H2′ and 23 × H2″ sugar ring protons, 5 × CH_3 of 5 × dT, 8×Arg-H^{β}, 8 × Arg-H^{δ}, 8 × Arg-H^{γ}, 8 × Leu-H^{β}, 4 × Leu-H^{γ}, 6 × CH_2 (aminohexyl linker), 1 × CH (aminohexyl linker), 6 × CH_2 (thiohexyl linker) 2 × Mal-H^{β}), 5.40–6.33 (m, 27H, 23 × H1′ sugar ring protons, 4 × H5 of dC), 7.25–8.41 (m, 30H, 30 × Ar-H from dG(× 7), dA(×14), dC(× 4) and dT(× 5)).

2.7.7. DC7 (5′ **2**-Mal-[LR]$_4$G-**5** 3′)

(72 nmol, yield 72%). MALDI-MS: *m/z* = 8740 $[M+H]^+$ (MW = 8739 calcd. for $[C_{296}H_{412}N_{115}O_{151}P_{23}S]$). ^{1}H NMR ($D_2O$ with TSP (0.01 μM), 400 MHz): δ 0.74–1.04 (m, 24H, Leu-H^{δ}), 1.24–3.26 (m, 124H, 23 × H2′ and 23 × H2″ sugar ring protons, 5 × CH_3 of 5 × dT, 8×Arg-H^{β}, 8 × Arg-H^{δ}, 8 × Arg-H^{γ}, 8 × Leu-H^{β}, 4 × Leu-H^{γ}, 6 × CH_2 (aminohexyl linker), 1 × CH (aminohexyl linker), 2 × Mal-H^{β}), 5.59–6.40 (m, 27H, 23 × H1′ sugar ring protons, 4 × H5 of dC), 7.38–8.41 (m, 30H, 30 × Ar-H from dG(× 7), dA(× 14), dC(× 4) and dT(× 5)).

2.7.8. DC8 (5′ **2**-Mal-[LRLRG]$_2$-**6** 3′)

(59 nmol, yield 59%). MALDI-MS: *m/z* = 7162 $[M+H]^+$ (MW = 7161 calcd. for $[C_{247}H_{353}N_{95}O_{120}P_{18}S]$). ^{1}H NMR ($D_2O$ with TSP (0.01 μM), 400 MHz): δ 0.76–1.02 (m, 24H, Leu-H^{δ}), 1.22–3.20 (m, 108H, 18 × H2′ and 18 × H2″ sugar ring protons, 3 × CH_3 of 3 × dT, 8×Arg-H^{β}, 8 × Arg-H^{δ}, 8 × Arg-H^{γ}, 8 × Leu-H^{β}, 4 × Leu-H^{γ}, 6 × CH_2 (aminohexyl linker), 1 × CH (aminohexyl linker), 6 × CH_2 (thiohexyl linker), 2 × Mal-H^{β}), 5.50–6.37 (m, 23H, 18 × H1′ sugar ring protons, 5 × H5 of dC), 7.27–8.39 (m, 25H, 25 × Ar-H from dG(× 3), dA(× 14), dC(× 5) and dT(× 3)).

2.7.9. DC9 (5′ **2**-Mal-[LRLRG]$_2$–**7** 3′)

(50 nmol, yield 50%). MALDI-MS: *m/z* = 7202 $[M+H]^+$ (MW = 7201 calcd. for $[C_{248}H_{353}N_{97}O_{120}P_{18}S]$). ^{1}H NMR ($D_2O$ with TSP (0.01 μM), 400 MHz): δ 0.76–1.02 (m, 24H, Leu-H^{δ}), 1.18–3.23 (m, 108H, 18 × H2′ and 18 × H2″ sugar ring protons, 3 × CH_3 of 3 × dT, 8×Arg-H^{β}, 8 × Arg-H^{δ}, 8 × Arg-H^{γ}, 8 × Leu-H^{β}, 4 × Leu-H^{γ}, 6 × CH_2 (aminohexyl linker), 1 × CH (aminohexyl linker), 6 × CH_2 (thiohexyl linker), 2 × Mal-H^{β}), 5.45–6.35 (m, 22H, 18 × H1′ sugar ring protons, 4 × H5 of dC), 7.28–8.41 (m, 25H, 25 × Ar-H from dG(× 4), dA(× 14), dC(× 4) and dT(× 3)).

2.7.10. DC10 (5′ **2**-Mal-[LRLRG]$_2$-**8** 3′)

(59 nmol, yield 59%). MALDI-MS: *m/z* = 8757 $[M+H]^+$ (MW = 8756 calcd. for $[C_{297}H_{415}N_{114}O_{152}P_{23}S]$). ^{1}H NMR ($D_2O$ with TSP (0.01 μM), 400 MHz): δ 0.76–0.97 (m, 24H, Leu-H^{δ}), 1.20–3.20 (m, 124H, 23 × H2′ and 23 × H2″ sugar ring protons, 5 × CH_3 of 5 × dT, 8×Arg-H^{β}, 8 × Arg-H^{δ}, 8 × Arg-H^{γ}, 8 × Leu-H^{β}, 4 × Leu-H^{γ}, 6 × CH_2 (aminohexyl linker), 1 × CH (aminohexyl linker), 6 × CH_2 (thiohexyl linker), 2 × Mal-H^{β}), 5.36–6.30 (m, 28H, 23 × H1′ sugar ring protons, 5 × H5 of dC), 7.14–8.39 (m, 30H, 30 × Ar-H from dG(× 6), dA(× 14), dC(× 5) and dT(× 5)).

2.7.11. DC11 (5′ **2**-Mal-[LRLRG]$_2$-**9** 3′)

(62 nmol, yield 62%). MALDI-MS: *m/z* = 8829 $[M+H]^+$ (MW = 8828 calcd. for $[C_{298}H_{415}N_{116}O_{154}P_{23}S]$). ^{1}H NMR ($D_2O$ with TSP (0.01 μM), 400 MHz): δ 0.71–1.01 (m, 24H, Leu-H^{δ}), 1.20–3.20 (m, 124H, 23 × H2′ and 23 × H2″ sugar ring protons, 5 × CH_3 of 5 × dT, 8×Arg-H^{β}, 8 × Arg-H^{δ}, 8 × Arg-H^{γ}, 8 × Leu-H^{β}, 4 × Leu-H^{γ}, 6 × CH_2 (aminohexyl linker), 1 × CH (aminohexyl linker), 6 × CH_2 (thiohexyl linker), 2 × Mal-H^{β}), 5.39–6.33 (m, 27H, 23 × H1′ sugar ring protons, 4 × H5 of dC), 7.24–8.32 (m, 28H, 28 × Ar-H from dG(× 9), dA(× 10), dC(× 4) and dT(× 5)).

2.8. Preparation of linearized plasmids and in vitro RNA transcripts

The detailed protocols for preparation of linearized plasmids p67YF0 and pHIV-2 as well as *in vitro* transcript of yeast $tRNA^{Phe}$ and 96-nts fragment of HIV-RNA (96-HIV-RNA) were reported earlier [30]. 3′-end labeling of RNA transcript with fluorescein isothiocyanate (FITC) was carried out using our previously published method [30].

2.9. Hybridization and cleavage of 3′-FITC $tRNA^{Phe}$ with DCs

The hybridization assays between 3′-FITC-$tRNA^{Phe}$ and one of the DCs, as well as subsequent quantitative data analysis were carried out as described earlier in Ref. [30].

Cleavage experiments were carried out for 3′-FITC labelled $tRNA^{Phe}$ (or 96-HIV-RNA) at concentration 1 μM (single turnover conditions) or 20 μM (multiple turnover conditions) plus one of the DCs at concentration 20 μM (single turnover conditions) or 10 μM (multiple turnover conditions) in 50 mM Tris–HCl pH 7.0, 0.2 M KCl, 1 mM EDTA in accordance with the previously reported protocol [30].

2.10. Molecular dynamics simulations

The MOE modelling package [35] was used to construct an $[LRLRG]_2$ peptide with attached linkers (*i.e.*, *N*-maleoyl-β-alanine, thiohexyl and aminohexyl groups) which were capped with phosphate groups simulating the attachment to oligodeoxyribonucleotides.

The system was built using the GAFF [36] and ff99SB [37] force fields for the linkers and peptide moieties respectively. Partial charges for the linkers were obtained using the R.E.D [38–40] server and AMBER12's *resp* module [41] *via* the RESP method [39] at the HF/6-31G* level of theory.

The molecular dynamics (MD) simulations were carried out using AMBER12's *pmemd* module [41] in five stages: (i) a 50 000 step minimization (steepest descent algorithm for the first 25 000 steps, conjugate gradient for the next 25 000); (ii) a 500 ps MD simulation in which the system was heated linearly from 0 K to the target temperature of 310 K; (iii) a 1 ns equilibration simulation at 310 K; (iv) a 1 ns simulation where a 20 kcal mol^{-1} $Å^{-2}$ harmonic distance restraint of 20.6 Å between the two end phosphorus atoms (simulating their likely distance when bound to $tRNA^{Phe}$) was slowly applied over 500 ps and then further equilibrated for another 500 ps; (v) a 10 ns production simulation with the distance restraint applied, sampling every 2 ps. The Generalized Born implicit solvation model with no cutoff [42–44] was used for all MD simulations. MD simulations used a time step of 2 fs and the SHAKE algorithm [45] was applied to constrain bonds involving hydrogens. The temperature was controlled using the Langevin thermostat with a collision frequency of 1 ps^{-1} [46].

2.11. Data processing and analysis

All hybridization and cleavage experiments were repeated 4–6 times independently. Experimental errors in measuring band intensities by Molecular Imager FX (Bio-Rad, USA) followed by gel images processing with *GelPro Analyzer* software did not exceed 5–7%. This was the estimated accuracy of cleavage data measurements. OriginPro 8.0 was used for data processing, and the binding constants K_a were evaluated using equation $K_a = \alpha/([DC](1-\alpha))$, where α is the binding extent and [DC] is the conjugate concentration. K_a values were expressed as mean ± SD (standard deviation).

3. Results and discussion

3.1. Design strategy

The overall design concept of the 'dual' peptidyl-oligonucleotide conjugates is shown schematically in Fig. 1A–B. The detailed secondary structure of $tRNA^{Phe}$ (*in-vitro* transcript) along with the binding regions for DCs and induced cleavage sites are illustrated in Fig. 1C. The key structural elements of the 'dual' peptidyl-oligonucleotide conjugates introduced here consist of two oligonucleotide recognition motifs connected by amphiphilic peptide (see Fig. 2), which acts both as a linker between two targeting oligonucleotides and as the catalytic moiety to promote hydrolytic cleavage of RNA at the adjacent sequence.

The isolated antisense recognition motifs do not contain a sufficient stretch of nucleotide residues to disrupt the native, thermodynamically stable $tRNA^{Phe}$ secondary structure [47–49]. However, when conjugated *via* a linker (Fig. 1A, dotted lines), these dual recognition motifs are expected to enhance considerably the likelihood of $tRNA^{Phe}$:DC heteroduplex formation, because multiple $tRNA^{Phe}$ structural elements are simultaneously disturbed. The recognition oligonucleotide elements were designed here in such a way as to allow a short region (**3** to **5** nucleotides) of single-stranded RNA (Fig. 1C) to remain in-between the hybridised RNA regions, thus leaving it susceptible to cleavage by the catalytic linker-peptide. An additional potential advantage of such a design could be that cleavage of the target $tRNA^{Phe}$ sequence at this location may potentially lead to catalytic turnover of the RNA substrate, as the binding weakens following cleavage. The number of Watson-Crick base pairs involved in the resulting heteroduplexes will be approximately halved after each successful cleavage event, thus weakening the hybridised complex. In this work, we aimed to investigate whether DC molecules can be released from their complex with tRNA following cleavage and attack the next RNA target sequence to be able to 'cleave and leave' again (Fig. 1A).

The synthesis of such constructs (see Tables 1 and 2 for oligonucleotide and peptide sequences, DC composition and nomenclature) was carried out using three consecutive steps. The catalytic peptides were synthesized using solid-phase peptide synthesis as previously described in Ref. [30]. The conjugation of the catalytic peptide to two oligonucleotide recognition motifs was carried out in solution in two subsequent stages, first *via* the *N*- and then *via* the C-terminus.

The core peptide sequences chosen for incorporation into DCs (*i.e.*, $[LR]_4G$, Mal-$[LR]_4G$ and Mal-$[LRLRG]_2$; see Fig. 2C) were based upon the RNA cleaving peptides $[LR]_4G$-$CONH_2$ and $[LRLRG]_2CONH_2$ that successfully demonstrated efficient cleavage of yeast $tRNA^{Phe}$, when covalently attached to a single 17-mer TΨC targeting oligonucleotide (pGATCGAACACAGGACCT) [30]. An additional glycine residue in the middle of the peptide chain of Mal-$[LRLRG]_2$ was incorporated, in an attempt to introduce additional flexibility between the two recognition sequences **A** and **B**, in order to improve the microenvironment for RNA cleavage, which can only occur *via* the 'in-line' mechanism [33,50–53]. Furthermore, incorporation of two additional linkers (*i.e.*, *N*-maleoyl-β-alanine and thiohexyl groups) into the structure of Mal-$[LR]_4G$ and Mal-$[LRLRG]_2$ allowed us to enhance further the conformational freedom of the catalytic peptide within the hybridised hybrid. Arginine-containing peptides are well known to bind to the phosphodiester backbone of RNA through their guanidinium functionality, which carries a positive charge at physiological pH. Furthermore, arginine residues are common in the active sites of several ribonuclease enzymes, where their role has been associated with the stabilisation of the phosphorane transition state *via* electrostatic interactions [54–56], which assist the delivery of the negatively-charged 2′-oxygen to the phosphorus, as well as acting as general-acid catalysts [57].

In order to investigate the effect of peptide length on RNA cleavage activity, in addition to the core peptide $[LR]_4G$, we also synthesized two analogous shorter peptides, $[LR]_2G$ and $[LR]_3G$, which contained fewer repeats of the leucine-arginine building block. The rationale behind this design was that a shorter peptide region may force the RNA to adopt a conformationally-strained, less thermodynamically stable DC:RNA hybridised complex, which could potentially promote DC dissociation and improve catalytic turnover. The catalytic peptides used in this research are listed in Table 2, along with the nomenclature of the corresponding DCs.

The oligonucleotides incorporated into the DCs were chosen based on their ability to hybridize with the $tRNA^{Phe}$ TΨC loop region or 3′-aminoacceptor stem (see red and blue ribbons, respectively, in Fig. 1C). In addition to modifying the peptide length between the core oligonucleotides GATCGAACACAG (within **1** or **2**) and TGGTGCGAATT (within **5**), additional oligonucleotides were designed to form single-stranded target regions of different size (5-, 4- or 3-nt) in the target $tRNA^{Phe}$ region (C61-G65), which may hypothetically affect the efficiency of the RNA strand cleavage (see Tables 1 and 2 for nomenclature). This was achieved by increasing the length of the recognition motif **A** (oligonucleotide **1**, Table 1) attached at the peptide *N*-terminus by one (GGATCGAACACAG/**3**) and two (TGGATCGAACACAG/**4**) nucleotide residues (underlined in the text and in Table 1). Therefore, upon DC:tRNA hybridization with these elongated recognition motifs, the number of unhybridised tRNA nucleotides in the target region (C61-G65) would be reduced from 5 to 4 and to 3, respectively. Previously, single-stranded target regions between 3 and 5 nucleoside residues have promoted hydrolytic RNA cleavage [58,59] presumably due to their ability to adopt the required 'in-line' geometry.

One of the fundamental problems with previous generations of POCs is their inability to leave their RNA target, following phosphodiester cleavage, in order for multiple catalytic events to occur. Therefore, it was important for us to test the hypothesis as to whether post-cleavage dissociation would be facilitated by replacement of the core oligonucleotide sequence **5** with a shorter recognition motif (*i.e.* CGAATT/**7**; Table 2) at the peptide C-terminus, or by incorporation of base mismatches into this shortened recognition motif (*i.e.* C***T***AA***C***T/**6**). Interestingly, the CTAACT motif, which was previously incorporated into a peptidyl-oligonucleotide conjugate, has been shown to display high levels of cleavage activity of such a POC against a HIV-1 RNA transcript with notable catalytic turnover [60,61]. To test this hypothesis, we aimed to assess the hybridization and cleavage performance of these shortened DC8 and DC9 conjugates.

Finally, as a compromise between the two hybridization extremes, two longer 11-mer oligonucleotides were also designed, one contained base mismatches (*i.e.* TGGTGC***T***AA***C***T/**8**), and another formed G-U 'wobble' base pairs on hybridization with $tRNA^{Phe}$ (*i.e.*TGGTGCG***GG***TT/**9**).

3.2. Synthesis of DCs

Peptides were synthesized by manual solid phase synthesis using the established Fmoc/^{t}Bu protocol. Peptides Mal-$[LR]_4G$ and Mal-$[LRLRG]_2$ were subject to an additional coupling procedure with *N*-maleoyl-β-alanine to allow subsequent modification with a thiol-bearing group. To allow for *N*- and *C*-terminal modifications after solid-phase synthesis of the peptides, both termini were left unprotected as an amine (or *N*-Maleoyl-β-alanine) and carboxylic acid, respectively.

DCs were synthesized by two different methods, which were selected based upon 3′- and 5′-terminal oligonucleotide modifications. **Method 1** (see Scheme S1, 'Supplementary Data' and Fig. 2A)

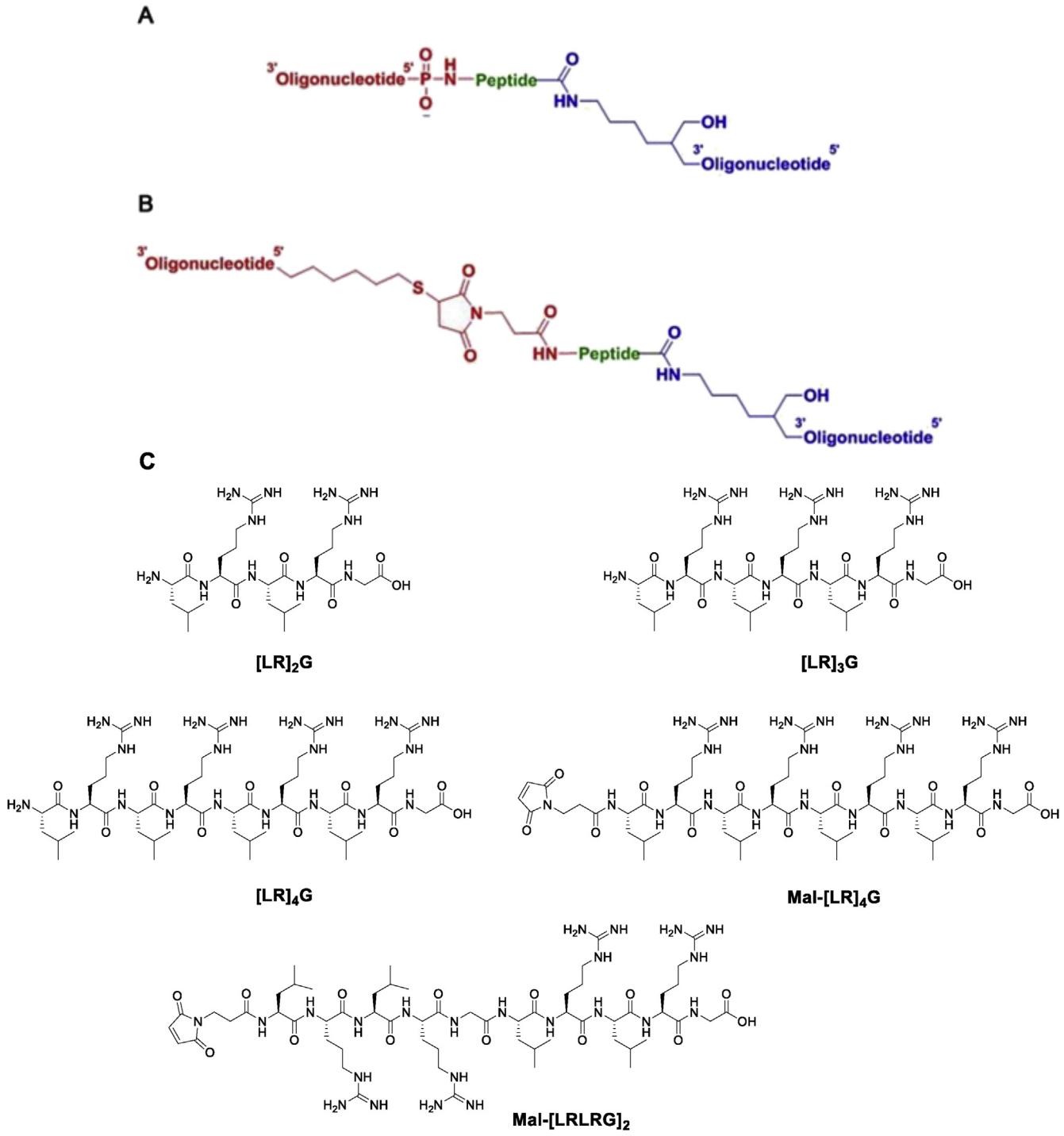

Fig. 2. General structures of dual conjugates DC1-DC3 (**A**) and DC4-DC11 (**B**) showing the conjugation regions between the catalytic peptide (green) and two flanking oligonucleotide recognition motifs A (red) and B (blue) along with their 5′- or 3′- modifications. (**C**). Chemical structures and nomenclature of peptides used in the synthesis of dual conjugates DC1 - DC11. (For interpretation of the references to colour in this figure legend, the reader is referred to the web version of this article.)

formed a phosphoramidate bond between a 5′-phosphate modified oligonucleotide and a peptide *N*-terminal amine [62]. The second oligonucleotide bearing a 3′- aminohexyl group was then attached *via* an amide bond-forming reaction at the peptide *C*-terminus (see Scheme S3, 'Supplementary Data'). **Method 2** (see Scheme S2, 'Supplementary Data' and Fig. 2B) utilized a thiol-maleimide 'click' reaction between a 5′-thiol modified oligonucleotide and a *N*-Maleoyl-β-alanine residue at the peptide *N*-terminus [63]. The second oligonucleotide was then attached using identical conditions to **Method 1**.

In **Method 1** (peptides $[LR]_2G$, $[LR]_3G$, $[LR]_4G$), the formation of the phosphoramidate bond between the 5′ terminal phosphate of the oligonucleotide (**1**) and the peptide *N*-terminus was achieved using the established method of Zarytova et al. [62], with appropriate adjustments due to the presence of a free *C*-terminal carboxylic acid. This required use of a DMSO-soluble

Table 1
Sequences, RNA binding site and nomenclature of recognition motifs.

Recognition Motif	Oligonucleotide	Sequence 5′→3′	Length, nts	Binding site
A	**1**	GATCGAACACAG [a]	12	49–60
A	**2**	GATCGAACACAG [b]	12	49–60
A	**3**	GGATCGAACACAG [b]	13	49–61
A	**4**	TGGATCGAACACAG [b]	14	49–62
B	**5**	TGGTGCGAATT [c]	11	66–76
B	**6**	C***T***AA***C***T [c,d]	6	66–71
B	**7**	CGAATT [c]	6	66–71
B	**8**	TGGTGC***T***AA***C***T [c,d]	11	66–76
B	**9**	TGGTGCG***GG***TT [c,d]	11	66–76

[a] 5′-terminal phosphate group at the 5′-end.
[b] Thiol-modification at the 5′-end.
[c] Aminohexyl linker at the 3′-end.
[d] Mismatches are marked in bold italics.

Table 2
Dual conjugate composition and nomenclature along with association constants (K_a) and total extent of $tRNA^{Phe}$ cleavage.

POC	Peptide	Oligo within recognition Motif A	Oligo within recognition Motif B	Target region length	K_a[a], 10^6 M^{-1}	Cleavage extent[b],%
DC1	$[LR]_2G$	**1**	**5**	5-nt	0.95 ± 1.1	0
DC2	$[LR]_3G$	**1**	**5**	5-nt	0.91 ± 0.9	0
DC3	$[LR]_4G$	**1**	**5**	5-nt	0.57 ± 0.4	0
DC4	Mal-$[LRLRG]_2$	**4**	**5**	3-nt	1.61 ± 0.2	<1[d]
DC5	Mal-$[LRLRG]_2$	**3**	**5**	4-nt	1.36 ± 0.2	<1[d]
DC6	Mal-$[LRLRG]_2$	**2**	**5**	5-nt	0.68 ± 0.1	100
DC7	Mal-$[LR]_4G$	**2**	**5**	5-nt	0.55 ± 0.1	40
DC8	Mal-$[LRLRG]_2$	**2**	**6**	5-nt	Negligible binding [c]	<1[d]
DC9	Mal-$[LRLRG]_2$	**2**	**7**	5-nt	Negligible binding [c]	<1[d]
DC10	Mal-$[LRLRG]_2$	**2**	**8**	5-nt	Negligible binding [c]	<1[d]
DC11	Mal-$[LRLRG]_2$	**2**	**9**	5-nt	Negligible binding [c]	<1[d]

[a] K_a was evaluated using equation $K_a = \alpha/[DC](1-\alpha)$, where α is the binding extent and [DC] is the conjugate concentration.
[b] Cleavage extent was determined as a ratio of fluorescence intensity measured in the RNA fragment(s) to the total fluorescence intensity applied onto the gel.
[c] Binding extent is less than 10%; K_a was estimated to be less than 1×10^3 M^{-1}.
[d] Cleavage extent did not exceed 1%.

cetyltrimethylammonium bromide salt of the oligonucleotide, along with activating agents 2,2′ dipyridyl disulphide, triphenylphosphine and 4-(dimethylamino)pyridine. In order to prevent peptide self-condensation, the phosphate group of the oligonucleotide was first pre-activated in anhydrous DMSO, and the activated oligonucleotide was isolated by precipitation in diethyl ether prior to addition of the peptide directly to the activated complex. Conjugation of oligonucleotide (**1**) to peptides $[LR]_2G$, $[LR]_3G$, $[LR]_4G$ gave similar yields between 80 and 90%. Prior to attachment of the second oligonucleotide motif (**5**) bearing a 3′-aminohexyl group, the identity and purity of the HPLC-purified 'single' conjugates were routinely confirmed by ^1H NMR and ^{31}P NMR to ensure correct product formation (see representative ^1H NMR spectra recorded for DC1 and its precursors in Fig. 3). The conjugation of the second recognition motif **B** *via* aminohexyl linker was achieved through the peptide *C*-terminal modification, which was carried out in 2-(*N*-morpholino)ethanesulfonic acid (MES) buffer (pH 6) with the water-soluble 1-Ethyl-3-(3-dimethylaminopropyl)carbodiimide (EDC) and *N*-hydroxy succinimide (NHS) activating agents. Reaction yields for attachment of the second oligonucleotide motifs to the 'single' peptidyl-oligonucleotide conjugates varied from 50 to 71%.

Method 2 (peptides Mal-$[LR]_4G$ and Mal-$[LRLRG]_2$) can be carried out in buffered aqueous solutions throughout [63,64]. The 5′-thiol modified oligonucleotides, supplied as protected disulphides were first reduced using *tris*(2-carboxyethyl)phosphine (TCEP) in phosphate-buffered saline (PBS) [64]. Unlike the reducing agent dithiothreitol (DTT), TCEP is not required to be removed from solution. Following disulfide reduction, the pH of the solution was raised (pH 7), and the peptide dissolved in DMSO was added dropwise. The reaction between the 5′-thiol and maleimide group was spontaneous [65], and the product yields for all 'single' conjugates synthesized in this manner were near quantitative (95–100%). Isolation of stereoisomers formed by this reaction was not carried out. Prior to attachment of the second oligonucleotides to generate DCs 4 to 11, the 'single' conjugates were purified by HPLC and routinely characterized by ^1H NMR to ensure correct product formation (data not shown here). However, due to the nature of the covalent attachment, ^{31}P NMR spectroscopy could not be used in this case to demonstrate attachment of the peptide to the oligonucleotide. The conjugation of the second recognition motif **B** (*i.e.* oligonucleotides **5**, **6**, **7**, **8** or **9**) was then achieved using the same approach as that described above for **Method 1**.

3.3. Characterization of DCs

The identity and purity of all 'dual' peptidyl-oligonucleotide conjugates were confirmed by IEX or RP-HPLC, Urea-PAGE, ^{31}P and/or ^1H NMR spectroscopy, and mass spectrometry. Precise analysis of ^1H NMR spectra is convoluted by the many overlapping signals in the peptide and oligonucleotide sugar ring regions (0.5–4.7 ppm). However, through comparison of the unconjugated oligonucleotides, intermediate 'single' peptidyl-oligonucleotide conjugates and the product dual peptidyl-oligonucleotide conjugates, we were able to confidently confirm the presence of the components and the correct ratio of oligonucleotide to peptide. As an example, Fig. 3 shows the ^1H NMR spectra of terminally-modified oligodeoxynucleotide starting materials (**1** and **5**), the intermediate peptidyl-oligonucleotide conjugation product of **1** with peptide $[LR]_2G$, and the final-product DC1. Following

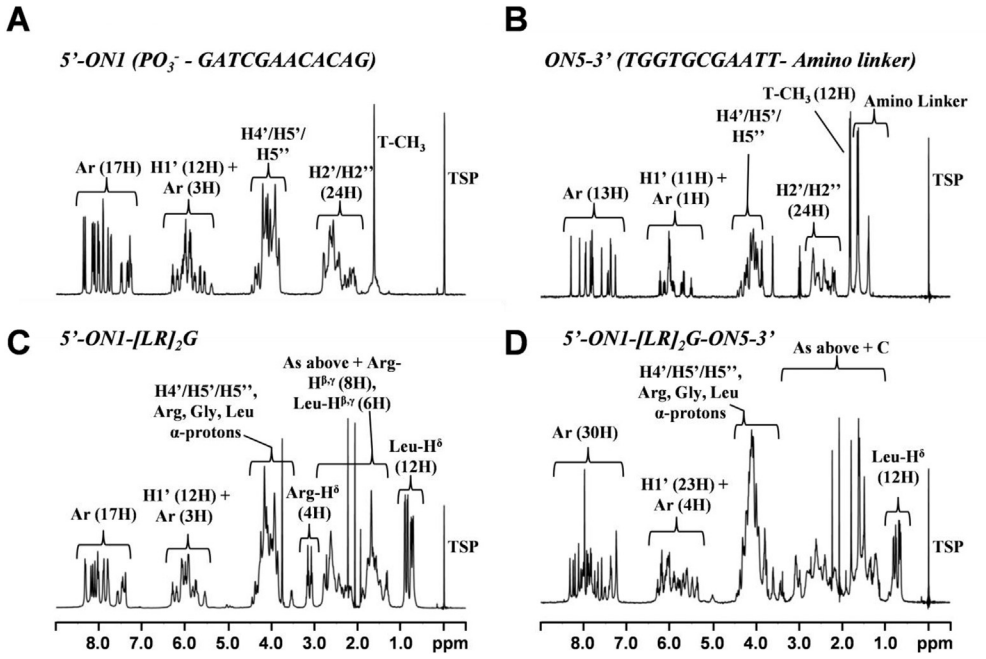

Fig. 3. Representative ^{1}H NMR spectra (400 MHz, Bruker Avance II+ 400) demonstrating a generic approach for characterization of 'single' and 'dual' peptidyl-oligonucleotide conjugates. NMR spectra of unconjugated oligonucleotides (**A** + **B**) along with intermediate (*i.e.* 'single') peptidyl-oligonucleotide conjugate (**C**) and 'dual' peptidyl-oligonucleotide conjugate DC1 (**D**). Integration of H3′/H4′/H5′/H5″ regions not carried out due to influence of water suppression.

attachment of peptide $[LR]_2G$ to **1**, some specific peptide signals in the resonance areas of 0.5–0.8, 3.0–3.4 and 3.6–3.7 ppm can be assigned to Leu-H^{δ}, Arg-H^{δ} and Gly-H^{α} protons, respectively. The considerable spectral overlap between the peptide protons and the oligonucleotide sugar ring protons made unambiguous assignment of the ^{1}H NMR signals difficult. However, through careful signal integration in the aromatic (7.3–8.4 ppm) and H1′/Ar-H5 (5.5–6.4 ppm) resonance areas of the oligonucleotide fragment, as well as those generated by Leu-H^{δ}, Arg-H^{δ} and Gly-H^{α} of the peptide component, it was possible to confirm 1:1 stoichiometric ratio of peptide to oligonucleotide.

Following attachment of the second oligodeoxynucleotide motif (**5**), the ^{1}H NMR spectrum of DC1 became even more complex and, consequently, only some signals could be fully characterized using conventional 1D NMR techniques. Again, the Leu-H^{δ} peptide signals were clearly observed; however, the Gly-H^{α} signal was shifted downfield and resided amongst the H4′/H5′/H5″ oligonucleotide sugar ring protons, due to the influence of the newly formed C-terminal amide bond. Other notable additions to the ^{1}H NMR spectrum of DC1 were the thymidine-CH_3 protons ($\times$ 4) of **5**, which formed clear singlets together with the T-CH_3 protons of **1**. However, precise integration of these resonances was not possible due to the interference from Arg-$H^{\beta,\gamma}$, Leu-$H^{\beta,\gamma}$ and H2/H2″ sugar ring protons of the oligonucleotide components. Incorporation of the second oligodeoxynucleotide motif was confirmed through integration of the aromatic (7.3–8.4 ppm) and H1′/Ar-H5 (5.5–6.4 ppm) regions. In the illustrated example, these showed an additional 13 and 12 proton signals, respectively, compared to the intermediate peptidyl-oligonucleotide conjugate (1-$[LR]_2G$). Again using these regions, it was possible to confirm the correct stoichiometric ratio (1:1) of peptide to oligonucleotide components. ^{1}H NMR spectra of all DCs were assigned in a similar fashion and all agreed with theoretical predictions.

^{31}P NMR analysis of DCs 1, 2 and 3 displayed the characteristic deshielding (5–6 ppm) of the terminal 5′-^{31}P resonance due to deshielding by the peptide *N*-terminus (see 'Materials and Methods'). However, ^{31}P NMR could not be used as a characterization tool for DCs 4 to 11 due to the nature of the 5′-thiol modification.

In mass spectrometry analysis, DCs were identified as mono- or di-sodium/potassium adducts with experimental masses in agreement with theoretical calculations (see 'Materials and Methods'). No fragmentation of DCs was observed under the experimental conditions used.

3.4. Hybridization of DCs to $tRNA^{Phe}$

Since cleavage of target RNA is expected to occur within the complementary complex formed between $tRNA^{Phe}$ and conjugate, the hybridization is an essential step preceding the RNA cleavage event.

The ability of DCs to hybridize with their target regions was determined by gel-shift analysis (see Fig. 4 and Table 2 for association constants). This was carried out by incubating 3′- FITC labelled $tRNA^{Phe}$ in a standard buffer (see 'Materials and Methods') with increasing concentrations of DCs, followed by analysis of the reaction mixtures by native 10% PAGE. Binding of the DC to 3′-FITC-$tRNA^{Phe}$ resulted in the formation of heteroduplexes with reduced electrophoretic mobility when compared to the unbound 3′-FITC-$tRNA^{Phe}$. Provided that 100% binding was observed binding constants could be estimated [49,51,52]. Previously, this technique has been used to identify oligonucleotides that bind with high efficiency to 3′-FITC-$tRNA^{Phe}$, such as: (i) a single 17-mer oligonucleotide recognition motif (GATCGAACACAGGACCT, K_a = $(7.0 \pm 1) \times 10^6$ M^{-1}) targeting $tRNA^{Phe}$ residues 44–61 encompassing variable and TΨC loops; and (ii) a 14-mer (TGGTGCGAATTCTG) targeting the 3′-ACCA overhang and acceptor stem [30,47,49]. In both cases, a single-stranded RNA region is required to initiate oligonucleotide:$tRNA^{Phe}$ hybridization, when only then can more structured RNA regions be unraveled. With the exception of oligonucleotides **6** and **7**, our oligonucleotides were designed here to target the same single-stranded

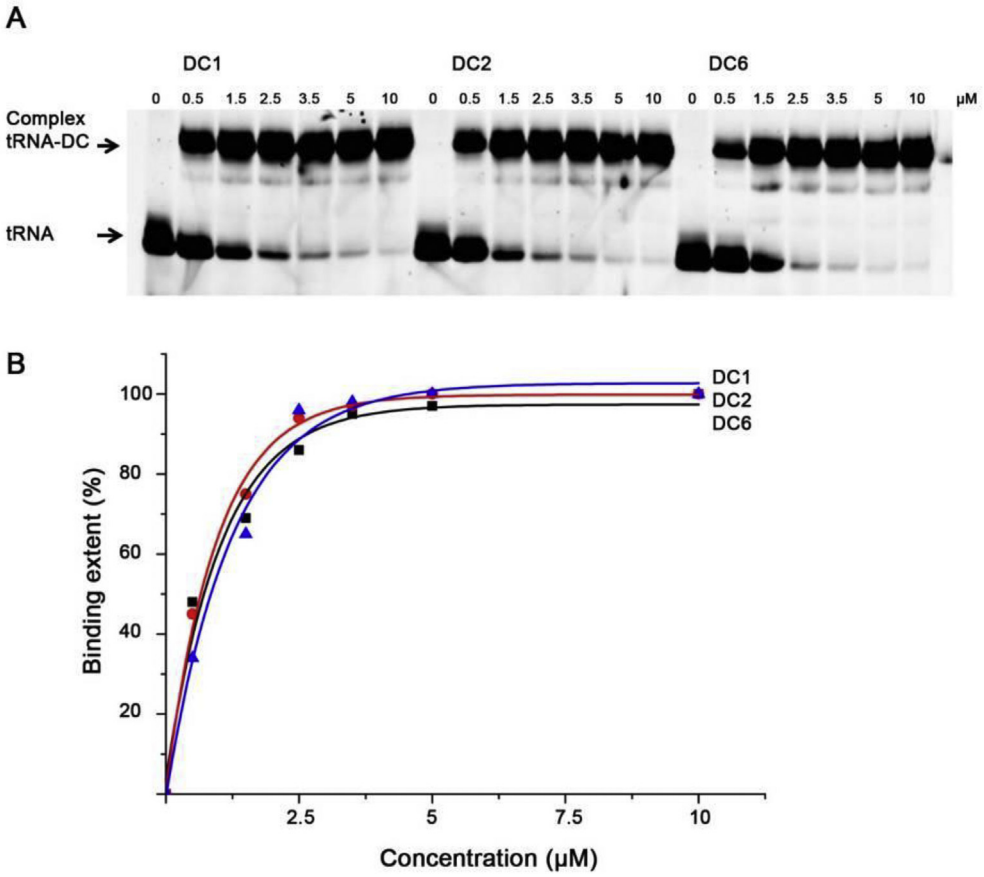

Fig. 4. Gel-shift analysis of hybridization of the DC1, DC2 and DC6 with 3′-FITC-tRNA^{Phe} (1 μM). **A**. Representative images of the 12% PAAG showing binding of the selected dual conjugates (DC1, DC2 and DC6) with 3′-FITC-tRNA^{Phe}. The conjugate type and concentrations are indicated at the top. Arrows show unbound 3′-FITC-tRNA^{Phe} and 3′-FITC-tRNA^{Phe}-conjugate complex. **B**. Secondary plot of the data shown in **A**.

initiation sites. However, due to the nature of the catalytic design of our DCs here, each oligonucleotide binding motif is shorter than those used previously (Fig. 1C). As expected, gel-shift analyses revealed that the unmodified oligonucleotides alone did not hybridize with their target RNA region under the conditions used (data not shown here). However, when operating jointly as part of the DC, both of these two oligonucleotide targeting motifs were able to mutually enhance the binding affinity of the conjugated molecule and hybridize with their target. As an example, demonstration of hybridization for DC1, DC2, and DC6 is shown (Fig. 4).

The dual conjugates studied here can be divided into two categories with respect to their ability to hybridize tRNA^{Phe}. Conjugates DC1 to DC7 from the first category demonstrated saturation binding to tRNA^{Phe} (Fig. 4 and Table 2) when 100% of the tRNA^{Phe} became hybridised to the DCs at concentrations above 5 μM. The association constant, K_a, calculated from this data, varied from 0.55 to 1.61 $\times$ 10^6 M^{-1}, showing that these conjugates had a strong affinity towards the target molecule (see Table 2). As expected, DC4, which forms two additional base-pairs (due to the lengthening of the Recognition Motif A by two nucleotides), exhibited the highest K_a value (K_a = 1.61 $\times$ 10^6 M^{-1}). In agreement with this, DC5 with one nucleotide less in its sequence bound to tRNA^{Phe} less tightly ($K_a = 1.36 \pm 0.2 \times 10^6$ M^{-1}), followed by DC6 with additional length reduction by another nucleotide residue ($K_a = 0.68 \pm 0.2 \times 10^6$ M^{-1}).

Among conjugates from the first category, which differed in the length of the peptide joining the two recognition motifs (DC1, DC2, DC3, DC6 and DC7**)** DC1, the shortest peptide displayed the highest binding constant (see Table 2). However, this result was not significantly greater than those obtained for DC6 and DC7, suggesting that the length and charge on the peptide (5-/7-/9-/10-/9-mer with +2/+3/+4/+4/+4, respectively) did not affect DC binding to a significant extent. This is in agreement with previous results for single conjugates, suggesting that the predominant force for hybridization is Watson and Crick base pairing and not electrostatic interactions between arginine residues and the phosphodiester backbone. As expected, the replacement of peptide *Mal*-$[LR]_4G$ (DC7) with *Mal*-$[LRLRG]_2$ (DC6) containing an extra glycine residue had only a very minor effect on the binding of the conjugate (Table 2). Additionally, DC**7**, containing identical antisense motifs to DC3, but with the replacement of a phosphoramidate linker, with a longer and more flexible thiol-maleimide linker showed no change in its binding constant. This suggests that an increased flexibility in this case did not contribute to or affect the binding ability of the DCs.

The second category of conjugates, which is represented by the conjugates DC8, DC9, DC10 and DC11 with truncated and/or mismatched recognition motif **B** (oligonucleotides **6**, **7**, **8** and **9**, respectively) showed very poor or negligible hybridization towards tRNA^{Phe} over a wide range of concentrations (up to 50 μM), with less than 10% extent of binding. Base mismatches and/or truncations of the RM **B** to miss out the 3′ overhang seem to be detrimental to binding efficiency, which is in a good agreement with previously obtained data [49,51,52].

Overall, binding of DC to RNA seemed to be driven solely by the oligonucleotide recognition motifs, as the peptide motifs seemed to

have negligible influence on the binding of the DCs to RNA.

3.5. Cleavage activity against of tRNA^{Phe}

Cleavage activities of the dual conjugates DC1-DC11 were screened at physiological pH 7.4 and temperature of 37 °C against 3′-FITC-tRNA^{Phe} (containing target regions complementary to the conjugate recognition motifs **A** and **B**) and 3′-FITC-HIV-RNA (which represents non-specific RNA target for the designed series of DCs). Tris-buffer was used here because it does not interfere with the RNA trans-esterification process [59,66,67]. It was supplemented with EDTA (1 mM) to minimise undesirable metal-ion induced RNA cleavage. Cleavage products were analysed by PAGE and identified by comparison with RNase T1 and imidazole tRNA^{Phe} hydrolysis ladders.

DC1, DC2 and DC3 appeared to be catalytically inactive towards the target tRNA^{Phe} sequence, possibly because the catalytic peptides ($[LR]_2G$, $[LR]_3G$ and $[LR]_4G$, respectively) were attached to the recognition motifs **A** and **B** (oligonucleotides **1** and **5**) *via* a zero-length phosphoramidate linker. This absence of catalytic activity may stem from the lack of essential conformational freedom upon hybridization of these conjugates to tRNA^{Phe}. The zero-length phosphoramidate linker at the 5′-end of DC1, DC2 and DC3 may restrict both peptide and the nucleotides, within the target site, from forming a favourable conformation for cleavage, leading to catalytic failure.

In order to investigate the plausibility of this hypothesis, the remaining dual conjugates DC4 - DC11 were assessed on their catalytic activity against tRNA^{Phe}, which incorporated extended and highly flexible *N*-maleoyl-β-alanine and thiol-hexyl linkers flanking the N-terminus of the catalytic peptide. The enhanced degree of conformational freedom had a considerable effect on their catalytic performance. Some of the conjugates from this series were highly catalytically active (Fig. 5), presumably due to increased flexibility of the heterocomplex around the target site. Indeed, conjugate DC7 induced 40% total cleavage of tRNA^{Phe} upon 24h incubation under identical conditions (*cf.* 0% RNA cleavage for DC1 - DC5; Table 2).

Furthermore, incorporation of an extra glycine residue into the catalytic peptide Mal-$[LRLRG]_2$ of DC6 promoted RNA cleavage even further and allowed this conjugate to achieve maximal catalytic activity (*i.e.*, 100%) in a much shorter incubation time (*i.e.*, 4h). The representative images of electrophoretic analysis of 3′-FITC-tRNA^{Phe} cleavage products are shown (Fig. 5) for DC6, DC7 and DC8 conjugates, and data summarised in Table 2.

The key role of conformational freedom in the catalytic cleavage of RNA by this class of dual conjugates was further confirmed by the reduced activity of two other conjugates (*i.e.*, DC5 and DC4) that contain the elongated recognition motif **A**, with 1 and 2 extra nucleotides, respectively, thus reducing the size of the RNA single-stranded target region. Indeed, narrowing the gap between the recognition motifs **A** and **B** within the complementary complex with tRNA^{Phe} led to a complete loss of the cleavage activity seen for these conjugates, presumably due to the conformational constraints, induced in the vicinity of the catalytic peptide.

However, our attempts to provide an even higher degree of freedom for the remaining dual conjugates (DC8, DC9, DC10 and DC12), to allow them to *'cleave and leave'* the hybridised complex, appeared to be detrimental for their catalytic performance (see Table 2). Indeed, these conjugates, which incorporated either shortened and/or mismatched recognition motif **B** (oligonucleotides **6**, **7**, **8** and **9**, respectively) showed negligible levels of binding affinity towards tRNA^{Phe} with an estimated K_a of less than 1×10^3 M^{-1}, with consequently poor catalytic activity (less than 1%). Clearly, the success of sequence-specific RNA cleavage relies on a very fine mechanistic balance between conformational tuning and base pair matching. Cleavage may be drastically suppressed by extremes, that is, by the lack of sufficient conformational freedom or by a disproportionate excess of it. This may be avoided, though, by careful structural consideration and rational structure-based design of the conjugates using, for example, multi-dimensional NMR spectroscopy and/or high level computational approaches.

3.6. Cleavage profiles and dynamics of tRNA^{Phe} cleavage induced by DC6 and DC7

The kinetics of tRNA^{Phe} cleavage induced by the most active dual conjugates (*i.e.*, DC6 and DC7) was evaluated from the time course of the cleavage reaction by measuring the extent of total tRNA cleavage against the incubation time (see Fig. 5). The kinetic curve for DC7 had a tendency to reach a plateau over a 24 h time period, which corresponded to 40% of overall tRNA^{Phe} cleavage. However, in the case of the DC6 conjugate, the plateau values reached 100% of total tRNA^{Phe} cleavage, with a complete disappearance of the intact tRNA^{Phe} band (Fig. 5A). Moreover, the kinetic curves measured for this dual conjugate reached a plateau in a much shorter period (*i.e.*, within 4 h), and further incubation (up to 8 h) led to a partial disappearance of the longer cleavage products, accompanied by accumulation of shorter RNA fragments.

Careful analysis of the tRNA^{Phe} cleavage sites identified for the most active conjugates DC7 and DC6 (see Fig. S4 and S5 in the 'Supplementary Data') revealed that even minor structural alterations in the peptide sequence (*i.e.*, an extra glycine residue in the Mal-$[LRLRG]_2$ present in the DC6 conjugate) could lead to a dramatic change in the RNA cleavage profile. Indeed, conjugate DC7 showed its ability to cleave tRNA^{Phe} both within the target region ^{61}CACAG^{65} (mainly at A62-C63 position) and outside this region at two Pyr-X sites (U9-A10 and C25-G26) (see Fig. 5A and Fig. S4). All identified sites induced by DC7 were recognized as primary cleavage sites, since the amounts of cleavage products[2] increase gradually over 24 h without any noticeable changes in the cleavage patterns.

Conjugate DC6 showed significantly more complicated and diverse cleavage patterns (see Fig. 5A and Fig. S5). One of the most interesting features of the DC6 conjugate seems to be its remarkable difference in base-selectivity of RNA cleavage seen for the target site against that observed for the distantly located regions. Indeed, at the target region ^{61}CACAG^{65} of the 3′-FITC-tRNA^{Phe}, DC6 attacked predominantly the A64-G65 position (60% over 24 h), with relatively slow cleavage kinetics, which reached a plateau only after 8 h of incubation. This was followed by a gradual accumulation of the minor products generated by cleavage at C63-A64 and A62-C63 sites (10% and 1%, respectively), which showed even slower cleavage kinetics. In contrast, outside the target region, DC6 exhibited predominately G–X cleavage specificity, thus mimicking T1-ribonuclease activity (see Fig. 1C for location of cleavage sites).

A pictorial description of the tRNA^{Phe} cleavage products induced by DC6 (**A**) along with a quantitative analysis of their accumulation over 24 h (**B**) is given in Fig. S5. In general, DC6 showed a 'natural' preference to cleave G-X phosphodiester bonds. However, when it became strongly bound to tRNA next to a single-stranded RNA region of 5 or more nucleotide residues, it tended to cleave any other linkages located in its close proximity (for example, A64-G65 and C63-A64).

Outside the targeted site, DC6 cleaved a number of G-X linkages

[2] Hereinafter cleavage products are labelled by the corresponding nucleotide residue located at the 5′- position from the cleavage point. For example, A64 product generated by cleavage at A64-G65 position corresponds to the 5′-G65-A76-3′ RNA fragment.

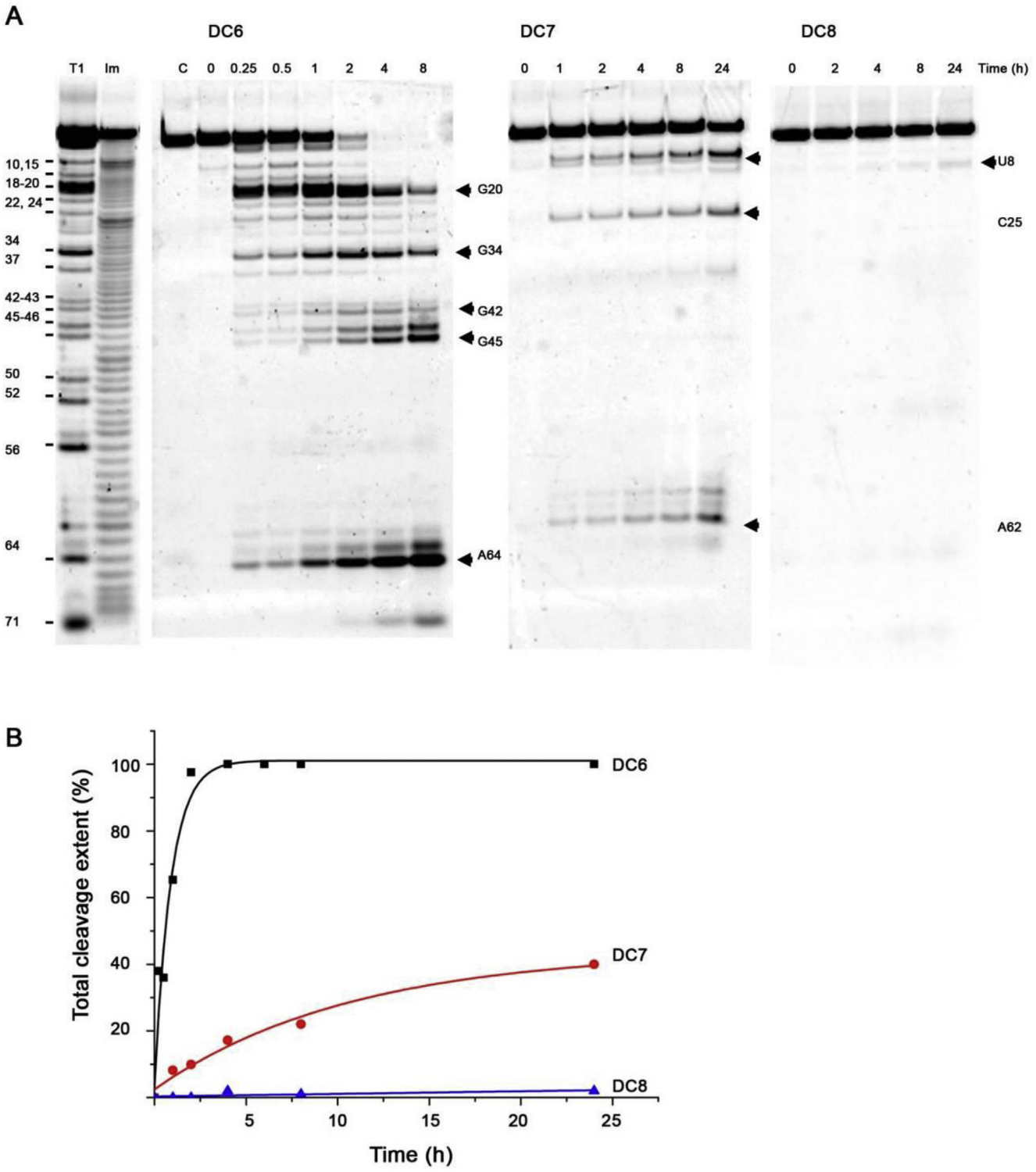

Fig. 5. Time courses of the cleavage reaction of 3′-FITC-tRNA^{Phe} with dual peptidyl-oligonucleotide conjugates (DC6, DC7 and DC8). **A**. Representative images of 12% PAAM/8 M urea gel after electrophoresis of 3′-FITC-tRNA^{Phe} cleavage products as a function of the incubation time. Lanes T1 and Im, partial 3′-FITC-tRNA^{Phe} digestion with RNase T1 and imidazole, respectively. Lane C, 3′-FITC-tRNA^{Phe} was incubated without conjugates for 24 h. 3′-FITC-tRNA^{Phe} (1 μM) was incubated with the conjugates (20 μM) at 37 °C for different time periods. Positions of RNA cleavage by RNase T1 and conjugates are shown on left and right respectively. **B**. Secondary plot of the data shown in **A** showing the total cleavage extent (%) plotted against the incubation time.

(see Fig. 1C) with a strong preference to regions G18-G20 > G34-A35 ≥ G45-U47. Cleavage at all other G-X sites was found to be insignificant (≤1%). The G20-A21 bond appears to be the most sensitive towards cleavage by the DC6 conjugate, as the corresponding cleavage product started to become detectable almost immediately (*i.e.*, after 25 min incubation with the conjugate). Cleavage at the G20-A21 site may be the consequence of the two main events.

(i) The hybridization of DC6 with tRNA may cause a destruction of the previously stable tertiary (L-form) tRNA molecule, which is accompanied by unfolding of the acceptor stem and T-stem [68]. This would facilitate the formation of the extended, gap-containing duplex and trigger the entire structural re-arrangement in the junction area, thus leading to increased flexibility of the D-stem and D-loop as well as the anticodon loop. The overall conformational flexibility of the entire tRNA structure seems to facilitate the interactions of the catalytic peptides with previously distant (in the intact L-form) regions of tRNA.

(ii) As a result of this enhanced structural flexibility, the G20-A21 bond appears to become the most favourable point to accommodate the 'in-line 'conformation, which is crucial for cleavage.

The cleavage of the other G-X bonds outside the target region (*i.e.,* G34-A35, G42-G43, G43-A44 and G45-G46 and G46-U47) may be governed mainly by their structural accessibility and occasional opportunities to approach the peptide during some random conformational fluctuations. The ability of these sites to adopt the 'in-line' conformations is another important factor to promote a successful cleavage event.

Since both DC6 and DC7 conjugates show efficient hybridization with $tRNA^{Phe}$ (*i.e.,* 100% at the reaction conditions) and contain exactly the same oligonucleotide recognition motifs, the marked differences in cleavage patterns and in the rates of RNA cleavage can be attributed solely to the additional glycine residue in the structure of DC6. This finding provides strong evidence that incorporation of a single amino acid into the peptide structure may completely switch cleavage specificity from Pyr-X to G-X. The results of this study are in agreement with the previous findings [30] that elongation of the peptide sequence from LRLRLRLRG to LRLR**G**LRLRG by insertion of only one extra amino acid in the middle of the peptide chain led to a dramatic increase in cleavage activity (from 24 ± 3% to 97± 8%). This discovery might be attributed to the gain in conformational freedom from the additional glycine residue, thus allowing the recognition motifs to optimise interactions with the target RNA sequence. It is well recognized that glycine residues play a crucial role in the active sites of many enzymes, as they provide a degree of conformational freedom to accommodate substrate binding and catalysis [69–72].

3.7. Evaluation of distances between the catalytic peptide and the main cleavage sites

We evaluated distances between the bridging phosphorus atoms of the C60-p-C61 site, which correspond to the region in the TΨC-arm of $tRNA^{Phe}$ opposite to the attachment point of the catalytic peptide, and the main RNA cleavage sites induced by DC6 and DC7 (Fig. 6 (**A**) and (**B**), respectively) using an available crystallographic structure of a yeast $tRNA^{Phe}$ [73] and the MOE software [35].

For the DC6:$tRNA^{Phe}$ complex, the distances to the main cleavage points vary (Table S1 in the 'Supplementary data') from 12.2 Å (C60-G18) to 54 Å (C60-G34). For the DC7:$tRNA^{Phe}$ complex, the distances to the main cleavage sites do not exceed 33 Å.

The longest distance between the phosphate atoms (*i.e.* points of attachment) and the guanidinium group nitrogen of one of the four arginine residues can be considered as an action radius for the catalytic peptide. Although approximate, the restraint biased MD simulations give us an indication that the peptide can potentially adopt some conformations where this distance could reach up to 36 Å. It is noted that this preliminary simulation model does not take into account the impact of the tRNA topology nor the effect of ionic interactions on the conformational flexibility of the peptide, however it does give us a basic estimate of its probable behaviour.

Fig. 6 (**C**) demonstrates representative conformations of the peptide which, if adopted, would allow almost all cleavage sites to be reached. Based on these evaluations, we can conclude that only one region (G34-A35) out of 9 main cleavage sites seems to be beyond the 'action radius' of the conjugate, as the distance was found to be 54 Å between this site and the bridging phosphorus atoms of the C60-p-C61 region within the intact $tRNA^{Phe}$ structure.

$tRNA^{Phe}$ is known to have significant conformational flexibility [74–76], which may allow considerable structural fluctuations due to the absence of the modified nucleotides in transcript $tRNA^{Phe}$, a lack of Mg^{2+} ions in the reaction mixture and some other factors that may significantly enhance the conformational freedom of $tRNA^{Phe}$. For example, as discussed earlier, binding of DC6 to $tRNA^{Phe}$ triggers unfolding of the TΨC-arm and amino acceptor stem, thus making the whole structure even more flexible and accessible for cleavage. The other major cleavage sites (G18-G19, G19-G20, G20-A21, G45-G46, G46-U47) seem to be located within this 'reactive radius', as the distance between these sites and the points of attachment of the peptide does not exceed 25.4 Å.

Possible mechanisms of tRNA cleavage induced by this type of bioconjugate were discussed previously [30,32,33,57] with a comprehensive coverage of both general *acid-base* catalysis *via* phosphodiester transesterification and *guanidinium-mediated* RNA cleavage.

A new attempt to further investigate the catalytic role of guanidinium groups in promoting transesterification was recently made [56]. The study shows that the hydrolysis of phosphodiester bonds is catalysed by synchronized action of two guanidine groups present in the same molecular structure. It has been shown that bifunctional chemical nucleases built upon diphenylmethane analogues bearing two di-guanidine functional groups were capable of cleaving 2-hydroxypropyl-*p*-nitrophenyl phosphate (an RNA mimic) *via* an *acid-base* mechanism, similar to that seen for RNase A. This catalysis was achieved by a cooperative proton transfer between the neutral guanidine group (general base) and protonated guanidinium residue (general acid). Interestingly, the functional properties of the guanidinium moiety associated with the positive charge were shown to play a dual role in catalysis by (i) coordinating the negatively charged phosphate group through an electrostatic interaction and (ii) acting as an electrophilic activator and hence, enhancing the transesterification reaction. The structural properties of the molecular scaffold between the guanidine residues played a crucial role in the catalytic cleavage of the RNA analogues. The success of the phosphodiester cleavage seemed to depend on a compromise between spatial separation of the guanidine groups, structural pre-organisation and flexibility. Molecular flexibility was shown to be an important factor in catalysis, presumably, due to a high increase in conformational freedom, which may allow the bifunctional catalyst to adapt to the substrate in the transition state. However, the accompanying entropic cost might be detrimental for the catalytic efficiency. Although generally valuable, these mechanistic studies [56], which were carried out in a mixture of organic solvents, can only be tentatively compared to the cleavage experiments performed against biologically relevant RNA in purely aqueous solutions at physiological pH values. Furthermore, the question concerning the fine *base-specific* mechanisms of RNA cleavage induced by the DCs remains unanswered.

3.8. Concentration dependences of $tRNA^{Phe}$ cleavage by DC6 and DC7

Since the conjugate DC6 (or DC7) was present in a 20-fold excess against $tRNA^{Phe}$ (*i.e.,* 20 μM DC6 against 1 μM $tRNA^{Phe}$), it remained

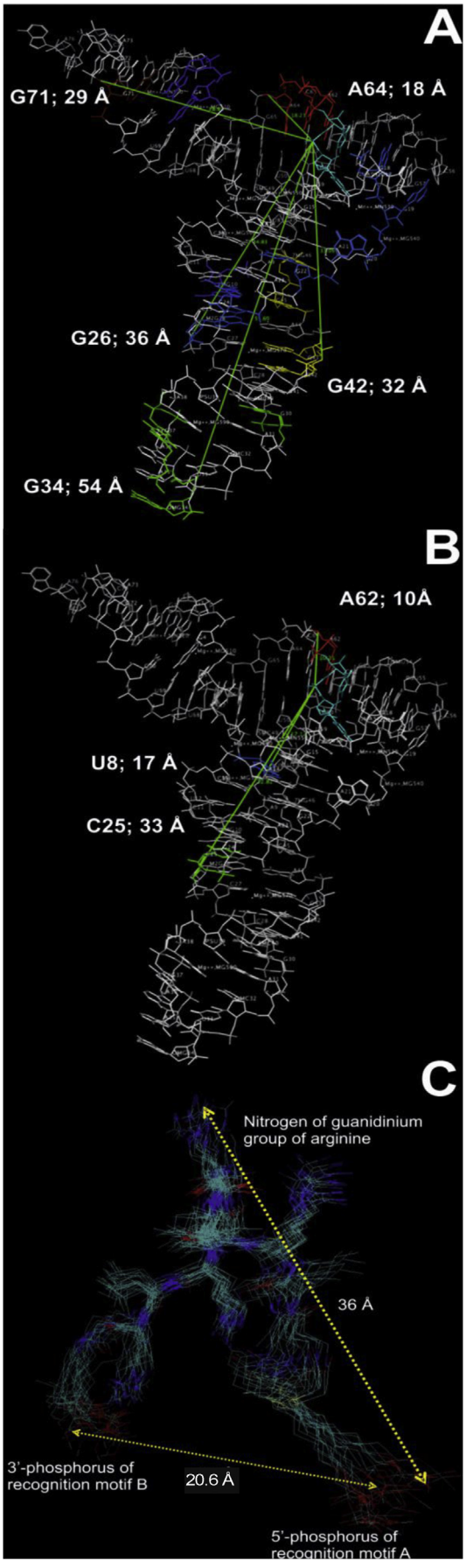

unclear how many molecules of DC6 (or DC7) may potentially participate in the cleavage of each $tRNA^{Phe}$ molecule. Although the conjugates were designed to bind $tRNA^{Phe}$ at 1:1 molar ratio, we cannot completely exclude the possibility of cooperative contribution of the additional conjugate molecules in RNA cleavage. Such formation of multimolecular complexes between RNA and chemical ribonucleases preceding the cleavage event has been experimentally demonstrated [77]. In order to investigate the mechanism of the $tRNA^{Phe}$ cleavage process, by the most active conjugates DC6 and DC7, we studied the cleavage profiles at their different concentrations. For DC6, we also looked at the cleavage kinetics in a 2-fold excess of tRNA (20 μM) over DC6 (10 μM).

The concentration dependences of $tRNA^{Phe}$ cleavage by both DC6 and DC7 conjugates exhibited sigmoidal behaviour, with a considerable lag period (Fig. 7) until the conjugate concentration reached 5 μM in the case of DC6, or until the concentration exceeded 10 μM for DC7. In contrast, the concentration dependence of binding to tRNA (Fig. 7B, dotted curves), estimated for both DC6 and DC7 conjugates, showed the usual hyperbolic character with curves reaching a plateau at around 7 μM in both cases.

The sigmoidal character of the cleavage curves and the presence of the lag period of the binding curves are consistent with some positive cooperativity taking place during the site-selective tRNA cleavage. This indicates that the complex formation might occur through several consecutive steps, similar to a process seen earlier for some oligonucleotides targeting the TΨC-loop [46].

There are at least two possible scenarios involving a cascade of subsequent events, which may explain (to a certain extent) the observed lag periods in the RNA cleavage by this class of conjugates. First, the conjugate may exist in solution as an ensemble of various conformational forms, and only when the effective concentration of the catalytically-active conformation of DC6 (or DC7) is achieved in the reaction mixture, does the RNA cleavage becomes detectable. This scenario assumes a quasi-stable complex within the *association-dissociation* process. It is based on a hypothesis that RNA cleavage can occur only within the 'productive' complex generated by the conjugate in its catalytically active form, which ultimately leads to a transformation of tRNA to its cleavage products. Another possible scenario may involve simultaneous interactions of two or more conjugate molecules with the same tRNA sequence, thus leading to formation of a 'reactive conformation'. According to this hypothesis, the first conjugate molecule is hybridised with the complementary sequence of the RNA target, whereas the second conjugate molecule or several molecular species are somehow involved in the catalysis through the formation of the 'productive' complex.

Both proposed scenarios could offer an explanation for the observed lag of cleavage against the binding curve (see Fig. 7). According to the first scenario, the effective cleavage of RNA is not seen in the conditions when the effective concentration of an 'active conformation' of DC6 (or DC7) is not sufficient for the cleavage to be detectable. According to the second scenario, the

Fig. 6. Structural evaluation of accessibility of the main cleavage sites by the catalytic peptide seen for the DC6:$tRNA^{Phe}$ and DC7:$tRNA^{Phe}$ complexes. Nucleotide residues from the C60-p-C61 region of the $tRNA^{Phe}$ are indicated in cyan. (**A**). Cleavage sites outside the target region within the DC6:$tRNA^{Phe}$ complex are shown in blue, green, yellow and red for the G3-G26, G30-37, G42-G46 and G71 clusters, respectively. (**B**) Cleavage sites outside the target region within the DC7:$tRNA^{Phe}$ complex are shown in blue, green and red for the nucleotide residues U8, C25 and A62, respectively. (**C**) Representative example conformations of the Mal-$[LRLRG]_2$ peptide generated *via* the MD simulations demonstrating the longest distance (thick dashed arrow) achieved between the phosphate atoms (i.e. points of attachment) and the guanidinium group nitrogen of one of the four arginine residues. The distance between the points of the peptide attachment within the hybridised complexes is indicated by the dotted arrow.

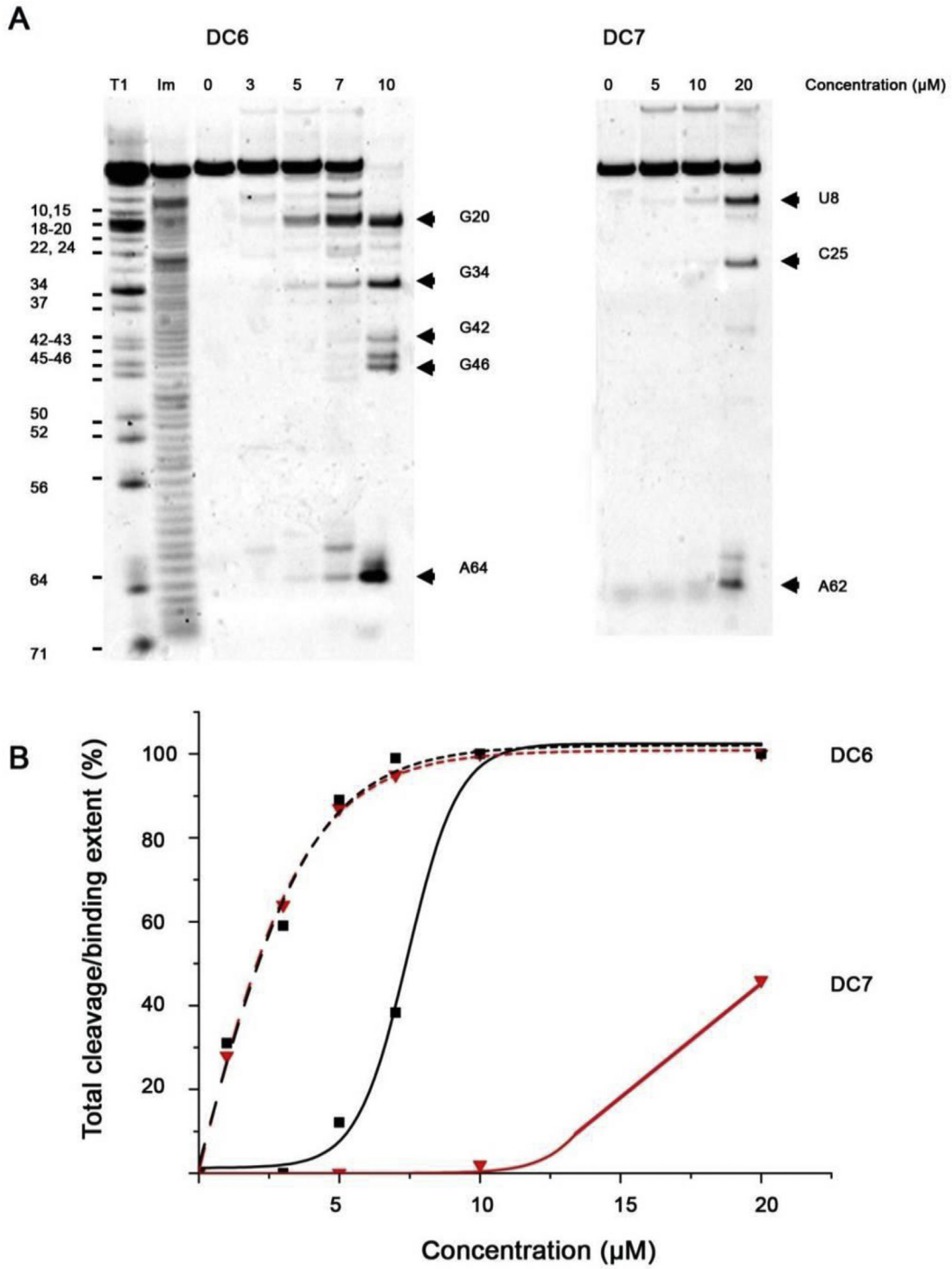

Fig. 7. Cleavage of 3′-FITC-tRNA^{Phe} with dual peptidyl-oligonucleotide conjugates DC6 and DC7 as a function of conjugate concentrations. **A**. Representative images of 12% PAAM/8 M urea gel after electrophoresis of 3′-FITC-tRNA^{Phe} cleavage products. Lanes T1 and Im, partial RNA digestion with RNase T1 and imidazole, respectively. 3′-FITC-tRNA^{Phe} (1 μM) was incubated with conjugates at various concentrations at 37 °C for 24 h. Positions of RNA cleavage by RNase T1 and conjugates are shown on left and right respectively. **B**. Concentration dependences of 3′-FITC-tRNA^{Phe} cleavage (solid lines) and binding (dotted lines) of 3′-FITC-tRNA^{Phe} with DC6 (squares) and DC7 (triangles) at 37 °C.

described mechanism can be activated after the conjugate concentration reaches 'critical' concentrations (*i.e.*, 5 and 10 μM for DC6 and DC7, respectively, in this example) needed for cooperative action.

The suggested hypotheses are also in agreement with our experimental data that neither DC6 nor DC7 cleave non-complementary RNA sequences and show absolute sequence-specificity (see Fig. S6, 'Supplementary Data'). 3′-FITC labelled 96-HIV-RNA (96-nts fragment of HIV-RNA, prepared by *in vitro* transcription) does not have any essential homology with yeast tRNA-^{Phe}, and was used here to evaluate the cleavage selectivity of DC6 and DC7 conjugates. Upon incubation of 3′-FITC-96-HIV-RNA

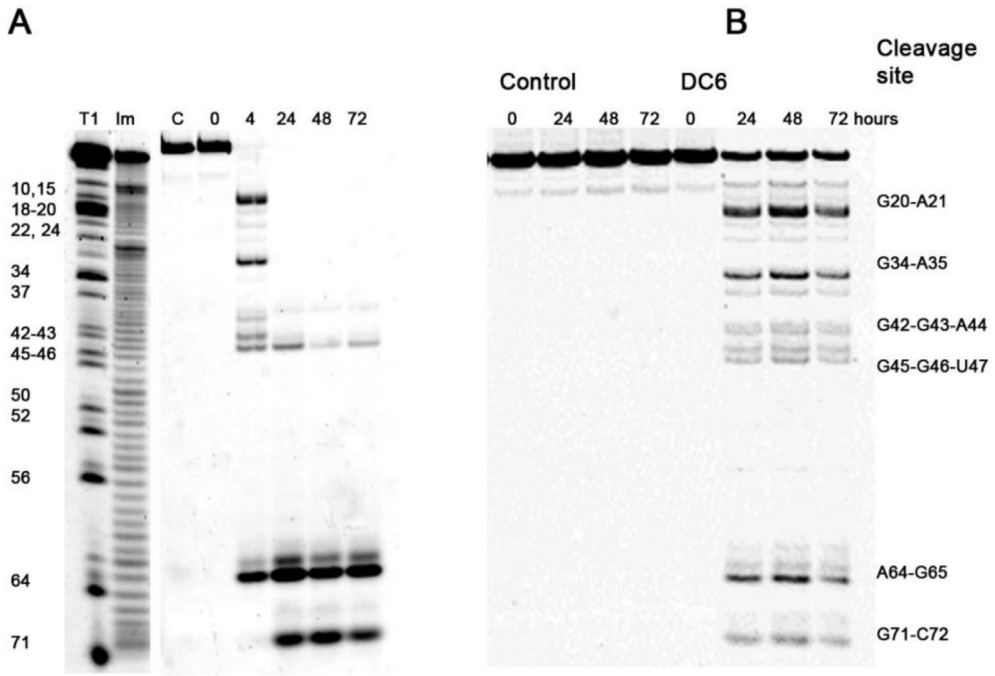

Fig. 8. Kinetics of 3′-FITC-tRNA^{Phe} cleavage with DC6 **A** in excess of DC6 (20 μM DC6, 1 μM 3′-FITC-tRNA^{Phe}) and **B** in excess of 3′-FITC-tRNA^{Phe} (10 μM DC6, 20 μM 3′-FITC-tRNA^{Phe}). Representative images of 12% PAAM/8 M urea gel after electrophoresis of 3′-FITC-tRNA^{Phe} cleavage products. Lanes T1 and Im, partial RNA digestion with RNase T1 and imidazole, respectively. Lane C, 3′-FITC-tRNA^{Phe} incubated in the absence of conjugate for 24 h. 3′-FITC-tRNA^{Phe} was incubated with DC6 at 37 °C. Positions of RNA cleavage RNase T1 are shown on the left.

(1 μM) with DC6 or DC7 (20 μM each), it remains intact with no cleavage being observed during 24 h incubation at 37 °C (Fig. S6). These results confirmed that (i) the designed dual conjugates work only as sequence-selective artificial ribonuclease and (ii) all cleavage events observed during the incubation of tRNA^{Phe} with DC6 or DC7 can occur only within the complementary complex between tRNA^{Phe} and dual conjugate.

3.9. *Cleavage of tRNA^{Phe} in excess with respect to DC6*

To explore further a plausible mechanism of RNA cleavage, we carried out the reaction in a 2-fold excess of tRNA^{Phe} (20 μM) with respect to DC6 (10 μM; Fig. 8). 50% of the tRNA^{Phe} cleavage was achieved in 24 h, and further incubation of tRNA^{Phe} in the presence of DC6 over next 72 h changed neither the overall extent of cleavage, nor the cleavage patterns (Fig. 8B).

Furthermore, the qualitative and quantitative distribution of the tRNA^{Phe} cleavage products were very similar to those seen for the 4 h reaction period when 20-fold excess of the conjugate was used (*cf.* tRNA^{Phe} at 1 μM and DC6 at 20 μM; Fig. 8A). This excludes neither the first scenario (insufficient concentrations of the catalytically active conjugate concentration) nor the second scenario (a necessity of multimeric catalytic complexes).

Although the total extent of tRNA^{Phe} cleavage reached was only 50% in the case of a 2-fold excess of RNA over DC6, we cannot completely exclude the possibility of the catalytic turnover of the reaction, especially in the case of scenario 2, with more than one conjugate molecule involved in the catalysis, and this aspect requires separate further investigation.

To conclude, the perception of the role that regulatory (non-protein coding) RNAs play in normal or pathologically compromised cells [3–8] led to a recognition of RNA as one of the most important biological targets for future therapeutic interventions. It was demonstrated that RNAs in cells are involved in the regulation of crucial biological functions, and thus an interference with their expression profiles or alteration of their specificity may play a pivotal role in progression of many pathological conditions (*e.g.* different types of cancer as well as cardiomyopathies and disorders of the central nervous system). With this in mind, we focus our research on development of a new generation of catalytically active bioconjugates capable of recognizing and destroying certain regulatory RNAs, which may trigger the discovery of new ways of switching intracellular signaling pathways from *'diseased'* to *'normal'*. Although this research is only the beginning of this challenging direction, our encouraging results obtained for the pilot model RNA systems may open new exciting avenues in the RNA targeting and inspire others to search for novel approaches in treatment of human pathophysiology. We anticipate that the next challenge in this area will be (i) to investigate whether these (or similar) catalytic bioconjugates are able to demonstrate a sufficient catalytic activity in cells and destroy cellular miRNAs in a selective and controlled manner. In the case of success, it will be crucial to subsequently evaluate (ii) the time-span of such induced miRNA silencing impact and (iii) assess whether or not this effect is sufficient to achieve an essential alteration in gene expression profile to reach a required level of therapeutic response.

4. Conclusion

A novel class of catalytic biomaterials with two oligonucleotide recognition motifs conjugated to an amphipathic peptide promoted hydrolytic cleavage of tRNA^{Phe} at the targeted site, adjacent to the sequence-specific hybridization. Two out of the eleven conjugates synthesized, differing in the length and structure of peptide, oligonucleotide recognition motifs and linkers, demonstrated high cleavage activity against tRNA^{Phe} and illuminated the structural requirements of sequence-specific catalysis.

(1) Highly flexible (*e.g.* *N*-maleoyl-β-alanine, thiol-hexyl) linkers between the oligonucleotide recognition motifs and the catalytic peptide were vital, in order to provide sufficient flexibility for the peptide to adopt a conformation favourable for successful RNA cleavage.
(2) Narrowing the gap between the two recognition motifs within the complementary complex with $tRNA^{Phe}$ led to a reduced size of RNA in targeted single-stranded target region, which may result in complete loss of catalytic activity.
(3) Addition of an extra glycine residue in the peptide sequence dramatically changed both the cleavage patterns and the extent of RNA cleavage.
(4) The success of sequence-specific RNA cleavage depended upon a fine mechanistic balance between conformational tuning and base pair matching in order to achieve the remarkably high RNA cleavage activity (*e.g.* 100% cleavage extent in 4 h), experimentally demonstrated in this work.

This study demonstrates the catalytic properties of novel supramolecular biomaterials against RNA molecules. This new methodology provides the strong position for future development of novel approaches for sequence-specific targeting of biologically-significant RNAs in order to facilitate the discovery of new selective therapeutics against viral genomic RNAs and specific messenger RNAs or miRNAs implicated in disease.

Author contributions

E.V.B., M.A.Z. and V.V.V. conceived the project. A.W. conducted the design, synthesis, purification and full characterization of the peptide and conjugate samples under the supervision of E.V.B. A.W. and Y.S. carried out the tRNA labelling, conducted gel-shift assays, analysed the hybridization data and co-wrote the corresponding parts of the manuscript. Y.S conducted the cleavage assays and associated molecular biology work under the supervision of M.A.Z. and E.V.B. Y.S. carried out MD simulations and analysed the data. K.K.B. and I.A. provided assistance with the calculations. E.V.B., M.A.Z. and V.V.V. co-wrote the paper and contributed to methodology development. All authors discussed the results and commented on the manuscript.

Disclosure of potential conflicts of interest

The authors declare no conflict of interest.

Acknowledgments

This research has been supported by the Russian Science Foundation (Grant No. 14-44-00068), EPSRC (Grant No. EP/G017905/1) and Collaborative Research Framework Agreement with SOLVAY (Work Program 2). The authors would like to thank Prof. David J. Clarke for fruitful discussions and helpful guidance throughout this work. We also thank Dr. Richard Bryce for providing access to the molecular modelling software and facilities as well as for useful advice during MD simulations. We are grateful to the National Mass Spectrometry Centre (Swansea, UK) for carrying out the mass spectrometry analysis of the peptide and conjugate samples.

Appendix A. Supplementary data

Supplementary data related to this article can be found at http://dx.doi.org/10.1016/j.biomaterials.2016.09.033.

References

[1] R.V. Chari, Targeted cancer therapy: conferring specificity to cytotoxic drugs, Acc. Chem. Res. 41 (2007) 98–107.
[2] G. Casi, D. Neri, Antibody–drug conjugates and small molecule–drug conjugates: opportunities and challenges for the development of selective anticancer cytotoxic agents, J. Med. Chem. 58 (2015) 8751–8761.
[3] M.V. Iorio, M. Ferracin, C.-G. Liu, A. Veronese, R. Spizzo, S. Sabbioni, E. Magri, M. Pedriali, M. Fabbri, M. Campiglio, S. Ménard, J.P. Palazzo, A. Rosenberg, P. Musiani, S. Volinia, I. Nenci, G.A. Calin, P. Querzoli, M. Negrini, C.M. Croce, MicroRNA gene expression deregulation in human breast Cancer, Cancer Res. 65 (2005) 7065–7070.
[4] M.V. Iorio, R. Visone, G. Di Leva, et al., MicroRNA signatures in human ovarian cancer, Cancer Res. 67 (18) (2007) 8699–8707.
[5] A. Markou, I. Sourvinou, P.A. Vorkas, G.M. Yousef, E. Lianidou, Clinical evaluation of microRNA expression profiling in non-small cell lung cancer, Lung Cancer 81 (2013) 388–396.
[6] E.M. Small, E.N. Olson, Pervasive roles of microRNSs in cardiovascular biology, Nature 469 (2011) 336–342.
[7] K. Ono, Y. Kuwabara, J.H. Han, MicroRNAs and cardiovascular diseases, FEBS J. 278 (2011) 1619–1633.
[8] P.T. Nelson, W.X. Wang, B.W. Rajeev, MicroRNAs (miRNAs) in neurodegenerative diseases, Brain Pathol. 18 (2008) 130–138.
[9] L.V. July, M. Akbari, T. Zellweger, E.C. Jones, S.L. Goldenberg, M.E. Gleave, Clusterin expression is significantly enhanced in prostate cancer cells following androgen withdrawal therapy, Prostate 50 (2002) 179–188.
[10] M. Gleave, H. Miyake, Use of antisense oligonucleotides targeting the cytoprotective gene, clusterin, to enhance androgen- and chemo-sensitivity in prostate cancer, World J. Urol. 23 (2005) 38–46.
[11] S.J. Le Grice, Targeting the HIV RNA genome: high-hanging fruit only needs a longer ladder, in: B.E. Torbett, D.S. Goodsell, D.D. Richman (Eds.), The Future of HIV-1 Therapeutics, Springer International Publishing, 2015, pp. 147–169.
[12] R.J. Scarborough, K.L. Adams, A. Daher, A. Gatignol, Effective inhibition of HIV-1 production by shRNAs and siRNAs targeting a highly conserved site in HIV-1 Gag RNA is optimized by evaluating alternative length formats, Antimicrob. Agents Chemother. 59 (9) (2015) 5297–5305.
[13] T.K. Warren, C.A. Whitehouse, J. Wells, L. Welch, A.E. Heald, J.S. Charleston, P. Sazani, S.P. Reid, P.L. Iversen, S. Bavari, A single phosphorodiamidate morpholino oligomer targeting VP24 protects rhesus monkeys against lethal Ebola virus infection, mBio 6 (2015).
[14] P.B. Jahrling, L.E. Hensley, K. Barrett, H.C. Lane, R.T. Davey, State-of-the-Art workshops on medical countermeasures potentially available for human use following accidental exposures to Ebola virus, J. Infect. Dis. 212 (suppl. 2) (2015) S84–S90.
[15] A.J. Hamilton, D.C. Baulcombe, A species of small antisense RNA in post-transcriptional gene silencing in plants, Science 286 (1999) 950–952.
[16] J.T. Marques, B.R.G. Williams, Activation of the mammalian immune system by siRNAs, Nat. Biotech. 23 (2005) 1399–1405.
[17] M. Sioud, Induction of inflammatory cytokines and interferon responses by double-stranded and single-stranded siRNAs is sequence-dependent and requires endosomal localization, J. Mol. Biol. 348 (2005) 1079–1090.
[18] R.L. Kanasty, K.A. Whitehead, A.J. Vegas, D.G. Anderson, Action and reaction: the biological response to siRNA and its delivery vehicles, Mol. Ther. 20 (2012) 513–524.
[19] A.A. Khan, D. Betel, M.L. Miller, C. Sander, C.S. Leslie, D.S. Marks, Transfection of small RNAs globally perturbs gene regulation by endogenous microRNAs, Nat. Biotech. 27 (2009) 549–555.
[20] K. Tiemann, J.J. Rossi, RNAi-based therapeutics–current status, challenges and prospects, EMBO Mol. Med. 1 (2009) 142–151.
[21] K.A. Whitehead, J.E. Dahlman, R.S. Langer, D.G. Anderson, Silencing or stimulation? siRNA delivery and the immune system, Ann. Rev. Chem. Biomol. Eng. 2 (2011) 77–96.
[22] F.Y. Xie, M.C. Woodle, P.Y. Lu, Harnessing in vivo siRNA delivery for drug discovery and therapeutic development, Drug Discov. Today 11 (2006) 67–73.
[23] D. Haussecker, The business of RNAi therapeutics in 2012, Mol. Ther. Nucleic Acids 1 (2012) e8.
[24] D. Jones, The long march of antisense, Nat. Rev. Drug Discov. 10 (2011) 401–402.
[25] R. Geary, B. Baker, S. Crooke, Clinical and preclinical pharmacokinetics and pharmacodynamics of mipomersen (Kynamro®): a second-generation antisense oligonucleotide inhibitor of apolipoprotein B, Clin. Pharmacokinet. 54 (2015) 133–146.
[26] R. Kole, A.R. Krainer, S. Altman, RNA therapeutics: beyond RNA interference and antisense oligonucleotides, Nat. Rev. Drug Discov. 11 (2012) 125–140.
[27] N.L. Mironova, D.V. Pyshnyi, E.M. Ivanova, M.A. Zenkova, H.J. Gross, V.V. Vlassov, Covalently attached oligodeoxyribonucleotides induce RNase activity of a short peptide and modulate its base specificity, Nucleic Acids Res. 32 (2004) 1928–1936.
[28] N.L. Mironova, D.V. Pyshnyi, D.V. Shtadler, A.A. Fedorova, V.V. Vlassov, M.A. Zenkova, RNase T1 mimicking artificial ribonuclease, Nucleic Acids Res. 35 (2007) 2356–2367.
[29] D.V. Pyshnyi, M. Repkova, S. Lokhov, E.M. Ivanova, A.G. Venyaminova, V. Zarytova, Oligonucleotide-peptide conjugates for RNA cleavage, Nucleos. Nucleot 16 (1997) 1571–1574.

[30] A. Williams, Y. Staroseletz, M.A. Zenkova, L. Jeannin, H. Aojula, E.V. Bichenkova, Peptidyl–oligonucleotide conjugates demonstrate efficient cleavage of RNA in a sequence-specific manner, Bioconjugate Chem. 26 (2015) 1129–1143.

[31] N.G. Beloglazova, M. Fabani, A.M. Zenkova, E.V. Bichenkova, N.N. Polushin, V.V. Sil'nikov, K.T. Douglas, V.V. Vlassov, Sequence-specific artificial ribonucleases. I. Bis-imidazole-containing oligonucleotide conjugates prepared using precursor-based strategy, Nucleic Acids Res. 32 (2004) 3887–3897.

[32] T. Niittymaki, H. Lonnberg, Artificial ribonucleases, Org. Biomol. Chem. 4 (2006) 15–25.

[33] H. Lonnberg, Cleavage of RNA phosphodiester bonds by small molecular entities: a mechanistic insight, Org. Biomol. Chem. 9 (2011) 1687–1703.

[34] I.Y. Serpokrylova, L.S. Koroleva, V.N. Sil'nikov, Design of peptide-oligonucleotide conjugates as site-specific artificial ribonucleases, FEBS J. 278 (2011) 337.

[35] Molecular Operating Environment (MOE), 2013.08; chemical computing group Inc., 1010 sherbooke st. West, Suite #910, Montreal, QC, Canada, H3A 2R7, 2016.

[36] J. Wang, R. Wolf, J. Caldwell, P. Kollamn, D. Case, Development and testing of a general Amber force field, J. Comput. Chem. 25 (2004) 1157–1174.

[37] V. Hornak, R. Abel, A. Okur, B. Strockbine, A. Roitberg, C. Simmerling, Comparison of multiple Amber force fields and development of improved, Proteins 65 (2006) 712–725.

[38] F.-Y. Dupradeau, A. Pigache, T. Zaffran, C. Savineau, R. Lelong, N. Grivel, D. Lelong, W. Rosanski, P. Cieplak, The R.E.D. tools: advances in RESP and ESP charge derivation and force field library building, Phys. Chem. Chem. Phys. 12 (2010) 7821–7839.

[39] C.I. Bayly, P. Cieplak, W. Cornell, P.A. Kollman, A well-behaved electrostatic potential based method using charge restraints for deriving atomic charges: the RESP model, J. Phys. Chem. 97 (1993) 10269–10280.

[40] Alex A. Granovsky, Firefly version 8, www http://classic.chem.msu.su/gran/firefly/index.html.

[41] D.A. Case, T.A. Darden, T.E. Cheatham III, C.L. Simmerling, J. Wang, R.E. Duke, R. Luo, R.C. Walker, W. Zhang, K.M. Merz, B. Roberts, S. Hayik, A. Roitberg, G. Seabra, J. Swails, A.W. Götz, I. Kolossváry, K.F. Wong, F. Paesani, J. Vanicek, R.M. Wolf, J. Liu, X. Wu, S.R. Brozell, T. Steinbrecher, H. Gohlke, Q. Cai, X. Ye, J. Wang, M.-J. Hsieh, G. Cui, D.R. Roe, D.H. Mathews, M.G. Seetin, R. Salomon-Ferrer, C. Sagui, V. Babin, T. Luchko, S. Gusarov, A. Kovalenko, P.A. Kollman, AMBER 12, University of California, San Francisco, 2012, 12.

[42] G.D. Hawkins, C.J. Cramer, D.G. Truhlar, Parametrized models of aqueous free energies of solvation based on pairwise descreening of solute atomic charges from a dielectric medium, J. Phys. Chem. 100 (1996) 19824–19839.

[43] G.D. Hawkins, C.J. Cramer, D.G. Truhlar, Pairwise solute descreening of solute charges from a dielectric medium, Chem. Phys. Lett. 246 (1995) 122–129.

[44] V. Tsui, D. Case, Theory and applications of the generalized Born solvation model in macromolecular simulations, Biopolym. Nucl. Acid. Sci. 56 (2001) 275–291.

[45] J.P. Ryckaert, G. Ciccotti, H. Berendsen, Numerical integration of the cartesian equations of motion of a system with constraints: molecular dynamics of n-alkanes, J. Comp. Phys. 23 (1977) 327.

[46] M.P. Allen, D.J. Tildesley, Computer Simulations of Liquids, first ed., Oxford University Press, Oxford, 1987.

[47] R.N. Serikov, V. Petyuk, Y. Vorobijev, V. Koval, O. Fedorova, V.V. Vlassov, V.A. Zenkova, Mechanism of antisense oligonucleotide interaction with natural RNAs, J. Biomol. Struct. Dyn. (2011) 27–50.

[48] V.A. Petyuk, M.A. Zenkova, R. Giege, V.V. Vlassov, Hybridization of antisense oligonucleotides with the 3′ part of $tRNA^{Phe}$, FEBS Lett. 444 (1999) 217–221.

[49] R.N. Serikov, V.V. Vlassov, M.A. Zenkova, Hybridization of antisense oligonucleotides with yeast tRNAPhe: factors determining the efficiency of interaction, Russ. Chem. Bull. Int. Ed. 51 (2002) 1156–1165.

[50] H. Astrom, R. Stromberg, Synthesis of new OBAN's and further studies on positioning of the catalytic group, Org. Biomol. Chem. 2 (2004) 1901–1907.

[51] U. Kaukinen, L. Bielecki, S. Mikkola, R.W. Adamiak, H. Lonnberg, The cleavage of phosphodiester bonds within small RNA bulges in the presence and absence of metal ion catalysts, J. Chem. Soc. Perkin Trans. 2 (2001) 1024–1031.

[52] D. Hüsken, G. Goodall, M.J.J. Blommers, W. Jahnke, J. Hall, R. Häner, H.E. Moser, Creating RNA Bulges: cleavage of RNA in RNA/DNA duplexes by metal ion catalysis, Biochemistry 35 (1996) 16591–16600.

[53] I.L. Kuznetsova, M.A. Zenkova, V.V. Vlassov, RNA bulges as targets for selective cleavage by metal ions and organic compounds, Russ. Chem. Rev. 76 (2007) 279–288.

[54] A.M. Piatek, M. Gray, E.V. Anslyn, Guanidinium groups act as general-acid catalysts in phosphoryl transfer Reactions: a two-proton inventory on a model system, J. Am. Chem. Soc. 126 (2004) 9878–9879.

[55] F.A. Cotton, E.E. Hazen, M.J. Legg, Staphylococcal nuclease: proposed mechanism of action based on structure of enzyme—thymidine 3′,5′-bisphosphate—calcium ion complex at 1.5-Å resolution, P. Natl. Sci. U. S. A. 76 (1979) 2551–2555.

[56] R. Salvio, L. Mandolini, C. Savelli, Guanidine–guanidinium cooperation in bifunctional artificial phosphodiesterases based on diphenylmethane spacers; gem-dialkyl effect on catalytic efficiency, J. Org. Chem. 78 (2013) 7259–7263.

[57] D.O. Corona-Martinez, O. Taran, A.K. Yatsimirsky, Mechanism of general acid-base catalysis in transesterification of an RNA model phosphodiester studied with strongly basic catalysts, Org. Biomol. Chem. 8 (2010) 873–880.

[58] I.L. Kuznetsova, M.A. Zenkova, H.J. Gross, V.V. Vlassov, Enhanced RNA cleavage within bulge-loops by an artificial ribonuclease, Nucleic Acids Res. 33 (2005) 1201–1212.

[59] I.L. Kuznetsova, M.A. Zenkova, V.V. Vlassov, Cleavage of RNA bulge loops by artificial Rnases, Russ. Chem. Bull. 55 (2006) 1284–1294.

[60] N.L. Mironova, D.V. Pyshnyi, E.M. Ivanova, V.F. Zarytova, M.A. Zenkova, H.J. Gross, V.V. Vlassov, Sequence-specific RNA cleavage by oligonucleotide-peptide conjugates, Russ. Chem. Bull. 51 (2002) 1177–1186.

[61] N.L. Mironova, D.V. Pyshnyi, D.V. Stadler, I.V. Prokudin, Y.I. Boutorine, E.M. Ivanova, M.A. Zenkova, H.J. Gross, V.V. Vlassov, G-specific rna-cleaving conjugates of short peptides and oligodeoxyribonucleotides, J. Biomol. Struct. Dyn. 23 (2006) 591–602.

[62] V.F. Zarytova, E.M. Ivanova, S.N. Yarmolyuk, I.V. Alekseeva, Synthesis of arginine-containing oligonucleotide-5'-N-peptides, Biopolim. i Kletka 4 (1988) 220–222.

[63] R.J. Pounder, M.J. Stanford, P. Brooks, S.P. Richards, A.P. Dove, Metal free thiol-maleimide 'Click' reaction as a mild functionalisation strategy for degradable polymers, Chem. Commun. (2008) 5158–5160.

[64] N.J. Ede, G.W. Tregear, J. Haralambidis, Routine preparation of thiol oligonucleotides: application to the synthesis of oligonucleotide-peptide hybrids, Bioconjugate Chem. 5 (1994) 373–378.

[65] J.A. Burns, J.C. Butler, J. Moran, G.M. Whitesides, Selective reduction of disulfides by tris(2-carboxyethyl)phosphine, J. Org. Chem. 56 (1991) 2648–2650.

[66] J. Hall, D. Hüsken, R. Haner, Towards artificial ribonucleases: the sequence-specific cleavage of RNA in a duplex, Nucleic Acids Res. 24 (1996) 3522–3526.

[67] Y. Jin, J.A. Cowan, Targeted cleavage of HIV Rev response element RNA by metallopeptide complexes, J. Am. Chem. Soc. 128 (2006) 410–411.

[68] V. Petyuk, M.A. Zenkova, R. Giege, V.V. Vlassov, Interaction of complementary oligonucleotides with 3′-end of tRNA(Phe), Nucleoside Nucleotides 18 (1999) 1459–2146.

[69] B.X. Yan, Y.Q. Sun, Glycine residues provide flexibility for enzyme active sites, J. Biol. Chem. 272 (1997) 3190–3194.

[70] G.J. Bartlett, C.T. Porter, N. Borkakoti, J.M. Thornton, Analysis of catalytic residues in enzyme active sites, J. Mol. Biol. 324 (2002) 105–121.

[71] M. Okoniewska, T. Tanaka, R.Y. Yada, The pepsin residue glycine-76 contributes to active-site loop flexibility and participates in catalysis, Biochem. J. 349 (2000) 169–177.

[72] M.K. Tiwari, R.K. Singh, R. Singh, M. Jeya, H. Zhao, J.K. Lee, Role of conserved glycine in zinc-dependent medium chain dehydrogenase/reductase superfamily, J. Biol. Chem. 287 (2012) 19429–19439.

[73] H. Shi, P.B. Moore, The crystal structure of yeast phenylalanine tRNA at 1.93 A resolution: a classic structure revisited, RNA 6 (2000) 1091–1105.

[74] X. Zhang, R.C. Walker, E.M. Phizicky, D.H. Mathews, Influence of sequence and covalent modifications on yeast tRNA dynamics, J. Chem. Theory Comput. 10 (8) (2014) 3473–3483.

[75] A. Matsumoto, M. Tomimoto, N. Go, Dynamical structure of transfer RNA studied by normal mode analysis, Eur. Biophys. J. 28 (1999) 369–379.

[76] M.W. Friederich, E. Vacano, P.J. Hagerman, Global flexibility of tertiary structure in RNA: yeast $tRNA^{Phe}$ as a model system, Proc. Natl. Acad. Sci. U. S. A. Biochem. 95 (1998) 3572–3577.

[77] N.A. Kovalev, D.A. Medvedeva, M.A. Zenkova, V.V. Vlassov, Cleavage of RNA by an amphiphilic compound lacking traditional catalytic groups, Bioorg. Chem. 36 (2008) 33–45.